

CAUSES AND EFFECTS OF VARIATION IN WRIST RANGE OF
MOTION: INVESTIGATING THE KINEMATICS OF THE PROXIMAL
CARPAL ROW

by

ZOE MACK

A thesis submitted to the
Department of Mechanical and Materials Engineering
in conformity with the requirements for
the degree of Master of Applied Science

Queen's University
Kingston, Ontario, Canada

June 2020

Copyright © Zoe Mack, 2020

Abstract

Due to the complex nature of the wrist, we still do not fully understand how the healthy wrist functions. There are few muscle insertions at the wrist, so bone motion is induced by passive ligaments and bone to bone contact, making carpal bone kinematics challenging to understand and model. This challenge is magnified by subject-specific variation in ligament properties and bone shape. Previous work has linked variation in carpal bone motion to changes in wrist flexibility, but these investigations have focused on the radial side of the wrist. Thus, many potential causes of variation in carpal motion patterns have yet to be thoroughly explored.

To further understand the causes and ramifications of variation in normal carpal kinematics, we performed two studies using a database of 3D *in vivo* carpal bone postures. For the first study, we investigated variation in carpal bone motion on the ulnar side of the wrist. Contrary to theories embedded in the literature, we found that the triquetrum and lunate did not move in synchrony across a variety of functional wrist movements. We also identified a relationship between motion of the triquetrum and wrist laxity during wrist movement from 20° of radial deviation to 20° of ulnar deviation. During this movement, the component of flexion-extension in the motion of the triquetrum increased with increased wrist flexibility. In our second study, we investigated the influence of scaphoid shape on wrist flexibility. We found that the first two principal components of scaphoid shape were correlated with wrist flexion and extension range of motion, respectively. We also found evidence that scaphoid posture may be independent of scaphoid shape. Scaphoid posture affected the amount of scaphoid rotation during wrist flexion and extension.

Finally, we discuss how we can apply our findings to the development and evaluation

of surgical techniques through two ongoing projects: simulating wrist motion in cadaveric specimens, and investigating how scaphoid shape impacts screw placement following scaphoid fracture. The findings from this work provide insights about the intricacies of carpal bone motion, a step towards explaining differential responses to injury and treatments with the potential to inform targeted, patient-specific interventions.

Co-Authorship

The thesis contains the original work of Zoe Mack, completed under the supervision of Dr. Michael J. Rainbow. Chapter 2 was prepared as a manuscript to be submitted to the *Journal of Hand Surgery*, with the support of co-authors Dr. Robin Kamal, Gordon Best, Dr. Scott Wolfe, and Dr. David Pichora. Components of this chapter have been presented as abstracts at a joint meeting of the International Society of Biomechanics and the American Society of Biomechanics in August 2019, and have been accepted for presentation at the Annual Meeting of the Canadian Orthopaedic Society in June 2020. Chapter 3 was prepared as a manuscript to be submitted to the *Journal of the Royal Society Interface*, with the support of co-authors Dr. Robin Kamal, Dr. Joseph Crisco, and Dr. David Pichora. Experimental design, data analysis, and writing of the manuscripts was completed by the author, with feedback on data analysis and editing of the manuscripts by the co-authors.

Acknowledgments

First of all, I would like to thank my supervisor, Dr. Michael Rainbow, for providing invaluable suggestions, guidance, and insights over the past two years. Thank you for sharing your enthusiasm and passion, whether you are discussing biomechanics or the “correct” usage of the word grill.

I would also like thank my co-authors. Dr. David Pichora, Dr. Robin Kamal, Dr. Scott Wolfe, and Dr. Joseph Crisco, your clinical insights alongside your thoughtful comments and feedback allowed me to see the value of this work beyond my computer screen. Gordon Best, thank you for your role in data collection and for your continued support of this project.

I am grateful for the support of Dr. Rick Sellens. Thank you for your suggestions and guidance during our wrist meetings, and for your troubleshooting assistance in the lab.

This work would not have been possible without the support of my lab mates: Erin Lee, Lauren Welte, Liam Rodgers, Mitchell Wheatley, and everyone else in McLaughlin 215. Aside from always being willing to answer my questions and help out, you made coming into work every day exciting, and helped me find the answers to questions I never knew that I had.

I am incredibly grateful for the love and support of my boyfriend, Ian Goode. Thank you for introducing me to the world of engineering, solving all of my IT problems, teaching me about 3D printing, and always being willing to lend a helping hand. From ski trips to 5 km portages, I will never forget our adventures over the past two years.

I also want to thank my close friends Brianna Aultman and Rebekah Price. Although you may have provided more distractions than help with regards to this thesis, your unwavering

support and encouragement led me to where I am today.

Thank you to all my friends at Queen Street Fitness for supporting me through tough workouts, always being willing to teach me something new, and celebrating my accomplishments inside and outside of the gym.

Perhaps most importantly, thank you to my family for providing love, advice, and never-ending encouragement. Thank you to my parents, Andrea and Gord, for always believing in me, and showing interest in my work. I also would like to thank my sister Sarah, for all of the stories from your menagerie that never failed to make me laugh. Finally, I want to thank my grandmother, Charlotte. The time I was able to spend with you taught be how to see the beauty in the world around me, and I wish that you could be here to celebrate this accomplishment with me.

Contents

Chapter 1: Introduction	1
1.1 Anatomy of the Wrist	1
1.2 Carpal Instability and Surgical Techniques	3
1.3 Theories of Carpal Bone Motion	6
1.3.1 Row Theories	7
1.3.2 Column Theories	8
1.3.3 Row and Column? Variability in Carpal Bone Motion	9
1.4 Measuring Carpal Bone Motion	10
1.4.1 Static X-ray	10
1.4.2 Optical Motion Tracking	11
1.4.3 Computed Tomography (CT)	11
1.4.4 Biplanar Videoradiography (BVR)	11
1.5 Summary and Objectives	12
Chapter 2: The Intercalated Segment: Does the Triquetrum Move in Synchrony with the Lunate?	14
2.1 Introduction	14
2.2 Methods/Materials	15
2.2.1 Subject Selection and Data Collection	15
2.2.2 Data Processing and Kinematic Analysis	16
2.3 Results	19
2.3.1 Wrist Positioning	19
2.3.2 Global Carpal Bone Motion	19
2.3.3 Intercarpal Rotation	20
2.3.4 Wrist Laxity	20
2.4 Discussion	22
Chapter 3: Influence of Scaphoid Morphology on Wrist Range of Motion	27
3.1 Introduction	27
3.2 Methods/Materials	29
3.2.1 Subject Selection and Data Collection	29
3.2.2 Image Processing	29
3.2.3 Principal Component Analysis	30
3.2.4 Bone Position and Contact Region Analysis	31
3.3 Results	31

3.3.1	Principal Component Analysis	31
3.3.2	Bone Position and Contact Region Analysis	32
3.3.3	Scaphoid Posture	35
3.4	Discussion	35
Chapter 4:	Discussion and Conclusions	40
Appendix A:	Simulated Wrist Motion Using Cadaveric Specimens	53
A.1	Optical Motion Tracking	53
A.2	Bead Implantation	55
A.2.1	Bead Implantation Procedure	55
Appendix B:	The Impact of Scaphoid Morphology on Screw Placement in the Scaphoid	58
B.0.1	Modelling Procedure	58
B.0.2	Safe Zone Calculation	58
B.0.3	Optimal Screw Placement	59
B.0.4	Cross-sectional Area	60
B.1	Preliminary Results	61
B.1.1	Principal Component 1: Scaphoid Size	61
B.1.2	Principal Component 2: Scaphoid Shape	61
B.1.3	Sensitivity	63

List of Tables

2.1	Average angle between the triquetrum-radius or scaphoid radius helical axis and the lunate-radius helical axis	20
-----	---	----

List of Figures

1.1	Two views of the human wrist	2
1.2	The ligaments of the wrist	3
1.3	Functional motions of the wrist	4
1.4	Carpal Instability: VISI and DISI	5
1.5	Theories of carpal bone motion	6
2.1	Wrist positioning during CT scanning	17
2.2	Radius-based anatomical coordinate system	18
2.3	Comparison of the lunate-radius and the triquetrum-radius helical axes during a hammering task	21
2.4	Comparison of the relative rotation between the lunate and triquetrum for a series of wrist motions	22
2.5	Orientation of the triquetrum-radius helical axis versus wrist flexibility	23
2.6	Orientation of the triquetrum-radius helical axis shifts upwards during Hammer 2 to 3	24
3.1	Scaphoid posture	32
3.2	Relative between principal components of scaphoid shape and passive ROM	33
3.3	Scaphoid shape variance	33
3.4	Rotation between the scaphoid and capitate or radius during wrist flexion and extension	34
3.5	Rotation of the scaphoid during wrist flexion and extension	36
3.6	Effect of scaphoid shape on relative motion between the scaphoid and capitate	37
A.1	3D printed clusters are used for mounting optical tracking markers.	53
A.2	CAD model of the cadaveric specimen	54
A.3	3D printed replica of the cadaveric specimen	54
B.1	Simulated scaphoids showing three standard deviations of shape	59
B.2	Computation of the safe insertion zone and optimal screw axis	59
B.3	Computation of cross-sectional area of the safe insertion zone	61
B.4	Location and orientation of the screw axis for 32 simulated scaphoids	62
B.5	Length of the optimally placed screw for simulated scaphoids	62
B.6	Safe screw insertion volume	63
B.7	2D cross-sectional area of the safe insertion zone	63
B.8	The minimal cross-sectional area of the safe insertion zone	64

Chapter 1

Introduction

1.1 Anatomy of the Wrist

The human wrist is a two degree-of-freedom joint which allows for relative motion between the radius and the metacarpals. This motion is facilitated by the movement of eight small, irregularly shaped carpal bones (Figure 1.1). The carpal bones are often classified into two rows: the proximal row, containing the scaphoid, lunate, and triquetrum and the distal row, which contains the hamate, capitate, trapezoid, and trapezium.

There are no muscle insertions on the proximal carpal row, so the motion of the scaphoid, lunate and triquetrum is governed by bone-to-bone contact and by the network of ligaments holding these bones in place (Figure 1.2). Intrinsic ligaments connect carpal bones to each other, while extrinsic ligaments connect the carpal bones to the radius, ulna, and metacarpals.

Motion at the wrist can be broken into flexion-extension (FE) and radial-ulnar deviation (RUD). For some functional tasks, these motions are combined to produce circumduction or motion along an oblique axis. One such motion, the dart thrower's motion, has important clinical significance because it is involved in a large number of functional movements, from activities as simple as drinking from a glass to more dynamic motions such as throwing, batting, and golf. This motion is completed along an oblique axis, with the wrist moving from radial extension to ulnar flexion [2], [3] (Figure 1.3).

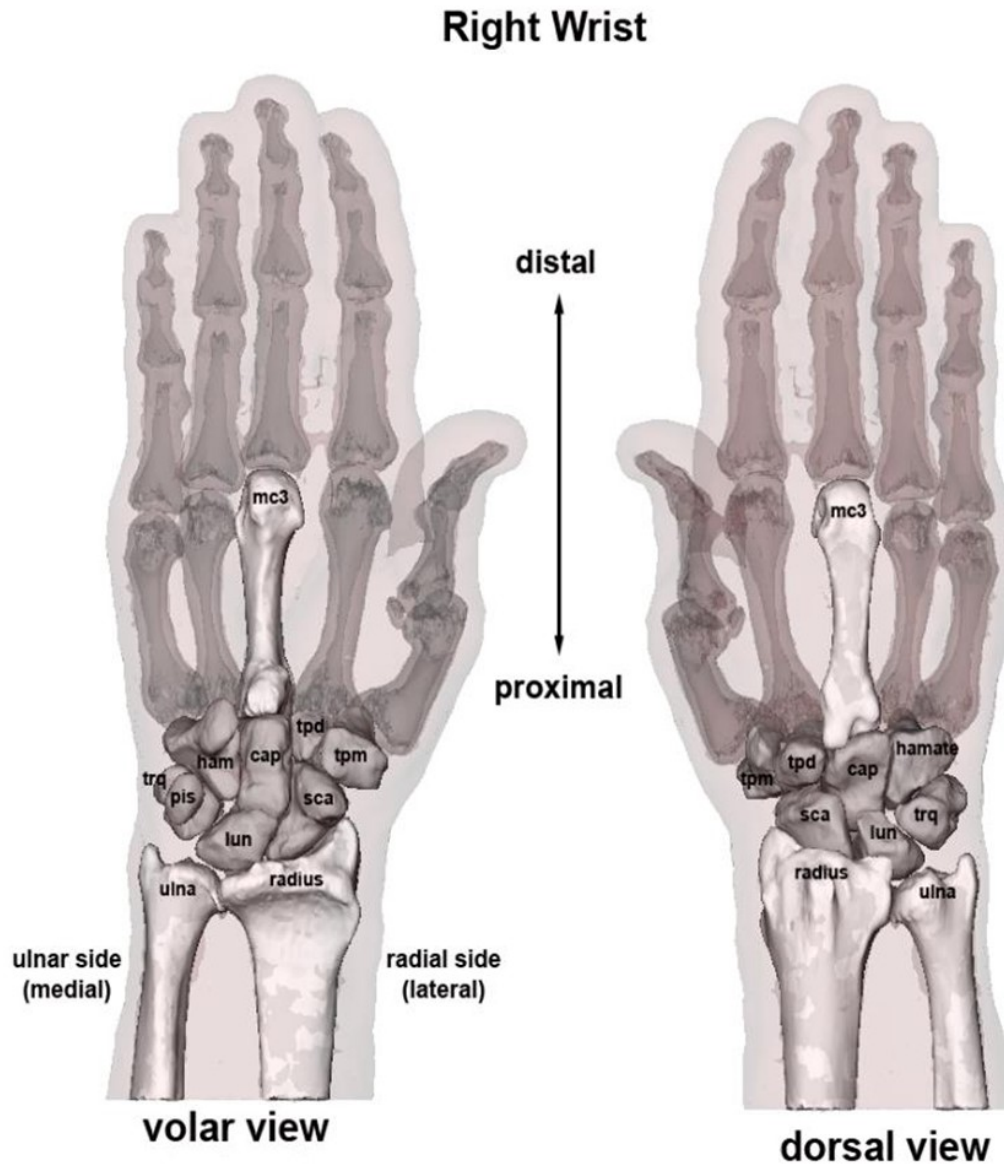


Figure 1.1: Two views of the human wrist, volar (palmer, or front) and dorsal (back). The distal carpal row consists of the hamate (ham), capitate (cap), trapezoid (tpd) and the trapezium (tpm) while the proximal row contains the triquetrum (trq), lunate (lun) and scaphoid (sca). The pisiform (pis) behaves similarly to a sesamoid bone, and articulates with the triquetrum. Image from [1] with permission.

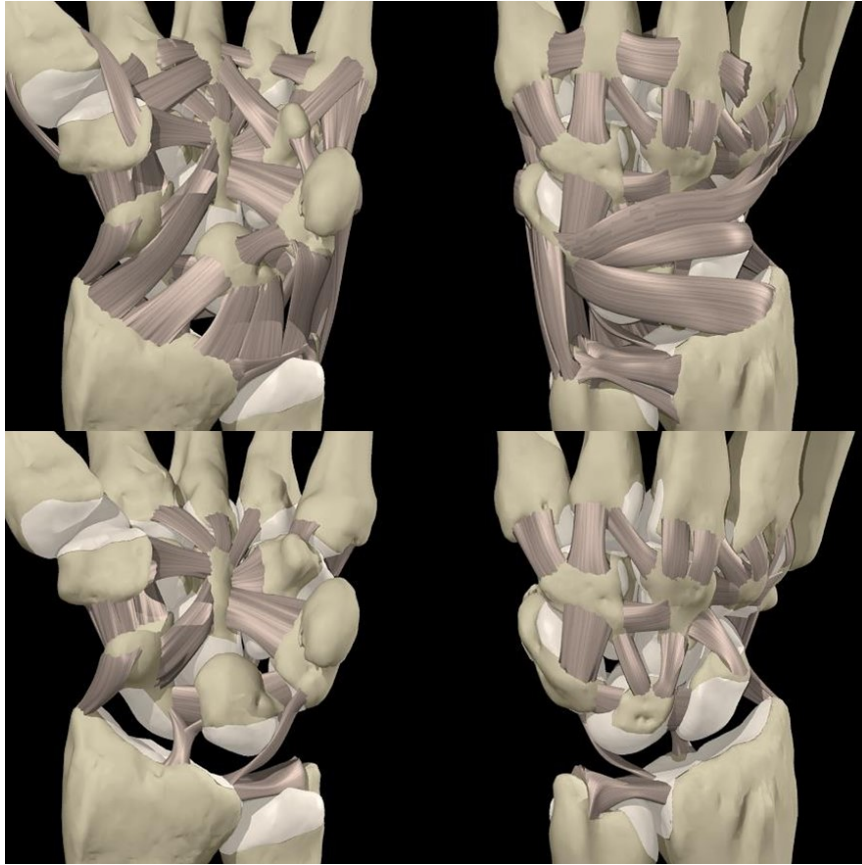


Figure 1.2: The ligaments of the wrist, volar (palmer) view (left) and dorsal (back) view (right). The extrinsic ligaments (top) connect the carpal bones to the radius, ulna, and metacarpals while the intrinsic ligaments (bottom) are found between carpal bones. Generated using: Interactive Hand 2000 © 2001 Primal Pictures

1.2 Carpal Instability and Surgical Techniques

The bones in the proximal carpal row are connected by two c-shaped ligaments, the scapholunate interosseous ligament (SLIL) between the scaphoid and lunate, and the lunotriquetral interosseous ligament which connects the lunate and the triquetrum (LTIL). Both ligaments can be subdivided into three sections (volar, proximal, and dorsal). The dorsal section of the SLIL is the thickest and strongest region, and is thought to be the primary stabilizer of the joint while the thinner volar region is theorized to provide rotational control [4]. The volar section of the LTIL is the thickest and strongest section of the ligament, with a weaker, thinner dorsal section [5]. Damage to the SLIL or LTIL can lead to carpal instability, which

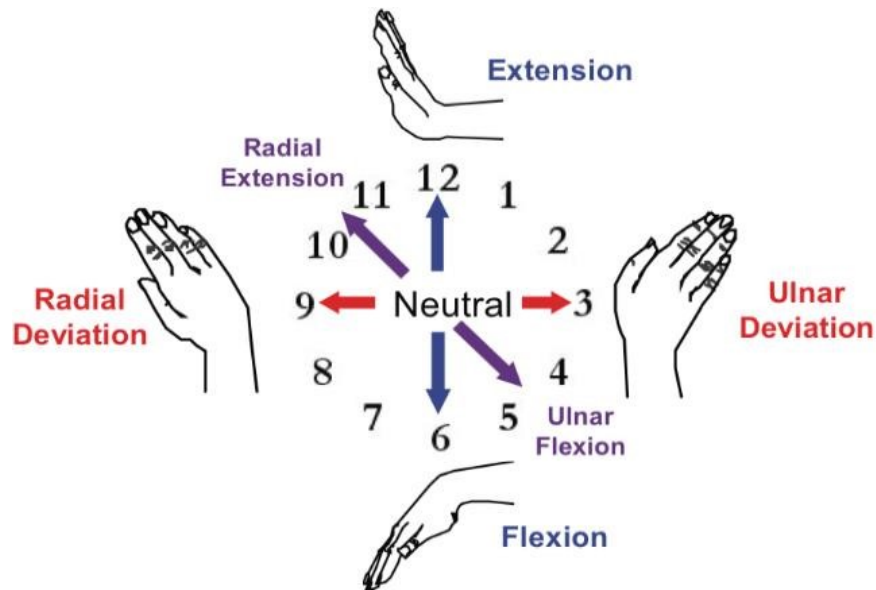


Figure 1.3: Functional motions of the wrist. The two primary motions, flexion-extension and radial-ulnar deviation can be combined to produce a dart thrower's motion, which follows a path from radial neutral to ulnar flexion. Image from [1] with permission.

often results in pain and difficulty performing activities of daily living.

Garcia-Elias proposed that the triquetrum and the scaphoid put opposing moments on the lunate, keeping it in a stable, centralized position [6]. If the SLIL and critical supporting ligaments are torn, the triquetrum pulls the lunate into extension via the thick, volar LTIL, causing dorsal intercalated segment instability (DISI). If the LTIL and critical supporting ligaments are torn, the scaphoid pulls the lunate into flexion via the thick, dorsal SLIL, a condition called volar intercalated segment instability (VISI). Thus, both ligaments must be intact to ensure the lunate stays in a stable position (Figure 1.4).

Injury to the SLIL is one of the most common carpal injuries, and can occur from simply falling on outstretched hand. If not treated, this leads to a predictable pattern of radiocarpal arthritis, starting at the radial styloid, progressing to the proximal scaphoid, and finally reaching the capitolunate joint [7]. Many procedures have been developed to reconstruct the scapholunate ligament, but none of them recreate the original anatomy, and outcomes are variable [8].

The reduction and association of the scaphoid and lunate (RASL) procedure involves

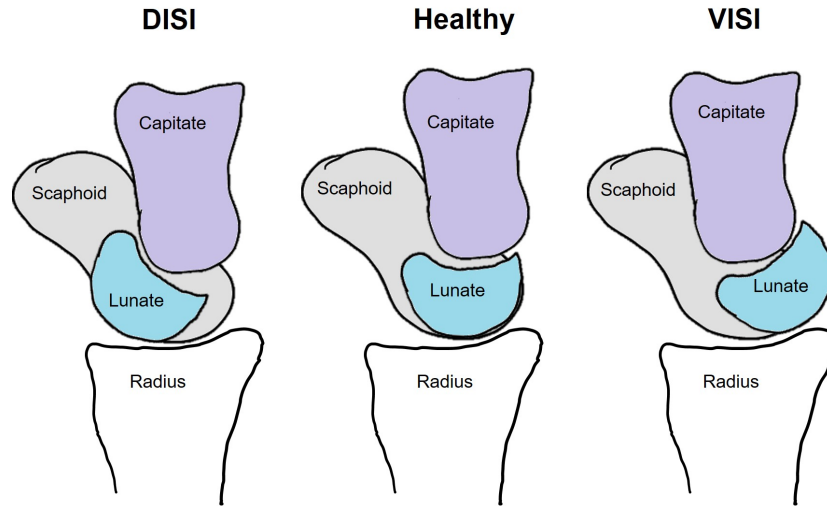


Figure 1.4: Right wrist, lateral view. Injury to the SLIL (left) results in DISI, or excessive lunate extension. Injury to the LTIL results in VISI (right), or excessive lunate flexion.

connecting the centre of the scaphoid to the centre of the lunate using a screw [9]. In the scapholunate axis method (SLAM), the gap between the scaphoid and the lunate is closed by passing a tendon graft from the lunate to the scaphoid and then wrapping the tendon dorsally to reconstruct the dorsal portion of the ligament [10]. Both of these procedures are partially based on the idea that the scaphoid and lunate move together about an axis aligned with the tendon or screw. However, our previous work shows that there is no consistent axis of rotation between the scaphoid, and in reality, the orientation and location of this rotation axis is quite variable [11]. Thus, these procedures are based on a flawed assumption. Neither procedure recreates the original structure of the ligament.

Other techniques used to reconstruct the scapholunate ligament include variations of the Brunelli procedure, and capsulodesis. In the Brunelli procedure, a tendon graft is passed through a hole drilled in the distal pole of the scaphoid to correct for excessive scaphoid flexion [12]. Capsulodesis involves suturing the joint capsule of the wrist to the scaphoid and lunate to correct for abnormal bone position and restrict bone movement [13].

None of these techniques reconstruct the original, c-shaped structure of the SLIL, which means that they are unlikely to restore the motion of the carpal bones observed prior to injury. To understand how carpal bone motion is affected by injury and by

reconstructive procedures, it is imperative that we first understand how the carpal bones function in a healthy wrist. This will provide a target for surgeons when performing ligament reconstruction.

1.3 Theories of Carpal Bone Motion

Wrist motion is facilitated by the movement of the eight carpal bones. Since these bones are small, irregularly shaped, and part of a passive structure, it becomes difficult to understand how the carpal bones move during wrist motion. Although the wrist has been studied extensively, to date we still have not developed a unified theory of carpal kinematics. Early descriptions of carpal kinematics generally either divided the carpal bones into rows or columns (Figure 1.5).

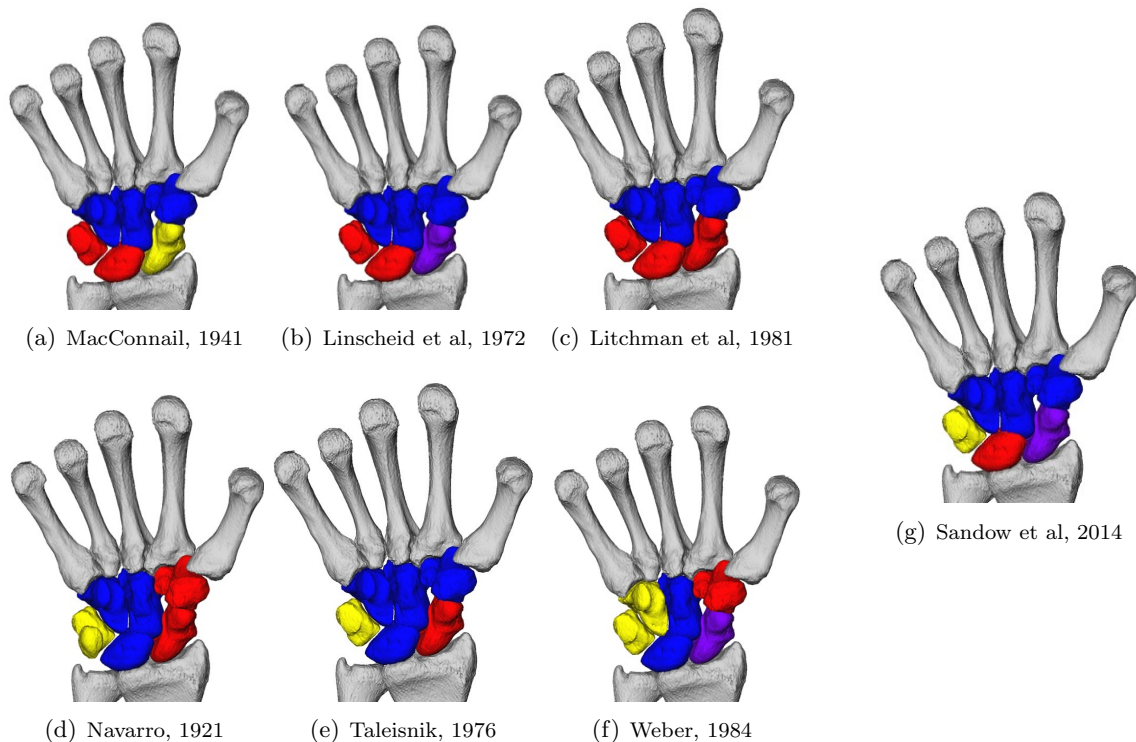


Figure 1.5: Row (top) and column (bottom) based theories of carpal bone motion. Colours are used to indicate the proposed bone groupings. The scaphoid is coloured purple to represent that in some theories, it belongs to multiple groups. For clarity, the pisiform is hidden where it is not included in the proposed model.

1.3.1 Row Theories

MacConnaill proposed that the two rows of carpal bones can be divided into three sections, each of which moves as a unit: the distal row, the scaphoid, and the remainder of the proximal row (Figure 1.5a) [14]. He observed that the scaphoid and capitate were locked together during wrist extension causing the scaphoid to move with the distal row, but during other wrist motions, the scaphoid tended to move with the proximal row. In extension, MacConnaill observed that the triquetrum was “screwed-in” to the hamate, but it was released in wrist flexion. MacConnaill described the tendency of the carpal bones to lock together and then release as a “screw clamp”. He observed that the carpus clamps down on the lunate during wrist extension to restrict motion in the proximal carpal row, and then releases the lunate in wrist flexion to allow more relative motion. This theory was further developed by Linscheid et al., who emphasized that the scaphoid acts a bridge between the proximal and distal rows to provide stability and allow the two rows to move together (Figure 1.5b) [15]. Linscheid et al. observed that the remainder of the proximal row (the lunate and triquetrum) moved together as an intercalated segment. During wrist radial-ular deviation, all the bones in the proximal carpal row tended to synchronously flex and extend. The triquetrum’s main role was believed to be an ulnar translation restraint for the proximal carpal row. Although still embedded in the literature today, Linscheid’s theory has never been directly tested through experimental means.

Lichtman et al. also believed that the carpal bones move as two distinct rows, but emphasized the ligamentous connections between the triquetrum and hamate and between the scaphoid and trapezium, which led to the conclusion that the carpus can be described as two connected rows, forming a ring (Figure 1.5c) [16]. Any disruption to this ring through bone fracture or ligament injury was believed to cause carpal instability. Lichtman et al. disagreed strongly with column-based theories, explaining that the lunate was very mobile compared to the capitate, so the wrist did not have a central column. They noticed that the entire proximal row moved as a unit, with small amounts of relative motion permitted between the lunate and scaphoid. However, more recent studies using three-dimensional

imaging have suggested that the proximal carpal row is more mobile than Lichtman et al. believed [17], especially towards the extremes of wrist range of motion [18].

1.3.2 Column Theories

Navarro subdivided the carpal bones into three columns: a central column responsible for wrist flexion and extension, a mobile lateral column, and a medial rotary column (Figure 1.5d) [19]. He believed that the central column allowed the wrist to flex and extend, while the medial and lateral columns provided support. This theory was later modified by Taleisnik, who concluded that the central column consisted of the entire distal carpal row, which moved as a single unit with the lunate (Figure 1.5e) [20]. The lateral mobile column consisted of only the scaphoid, while the medial rotary column consisted of only the triquetrum. The scaphoid stabilized the wrist by connecting the proximal and distal rows, while the triquetrum rotated against the hamate. Taleisnik observed that the scaphoid and the lunate moved together in flexion and extension, but that the scaphoid flexed more than the lunate during wrist flexion, providing evidence of relative motion between the bones in the proximal carpal row.

Weber also believed that the carpus could be split into three columns, but subdivided the carpal bones differently than Navarro and Taleisnik. In Weber's theory, the carpus was split into a central force bearing column containing the lunate and capitate, a thumb axis containing the trapezium and trapezoid, and a lateral control column consisting of the triquetrum and the hamate (Figure 1.5f) [21]. The scaphoid was split between the force bearing column and the thumb axis, with the distal two-thirds used for load-bearing. Weber believed that the interaction between the triquetrum and the hamate governed the movement of the bones in the proximal carpal row during wrist motion. He also reported that the bones of the proximal carpal row did not move with the wrist (measured as the motion of the third metacarpal relative to the radius) during radial-ulnar deviation. Instead, the scaphoid and lunate tended to flex in wrist radial deviation and extend in wrist ulnar deviation, an action he believed was driven by the triquetrum. Finally, Weber noted that

the strength of the interosseous ligaments in the proximal carpal row, reporting that motion between the proximal carpal bones was severely restricted causing them to move together, despite believing that the wrist functions as a series of columns.

1.3.3 Row and Column? Variability in Carpal Bone Motion

Recently, Sandow et al. proposed a new theory of carpal bone motion, which blends the row and column theories (Figure 1.5g) [22]. In this model, the carpus is broken into four segments. The distal carpal row, or distal segment, moves as a solid unit, the scaphoid makes up the lateral segment, the lunate is the proximal segment, and the triquetrum is the medial segment. The lunate and capitate form a central, stable column, while the scaphoid acts as a supporting lateral column to the remainder of the carpus, and mostly moves with the lunate. The triquetrum acts as an ulnar translation and flexion restraint for the lunate.

Although these theories may seem contradictory, there are several common ideas. It is well accepted that the distal row moves together as rigid unit in the same direction as wrist motion. However, proposed motion of the bones in the proximal row is much more variable. In some theories, all the bones of the proximal row move together, in others, the scaphoid and lunate move together, while in others, the lunate and triquetrum move synchronously. Many theories highlight the interaction between the triquetrum and the hamate, but it is still unclear whether this interaction is driving proximal bone motion as proposed by Weber [21], or simply acting as a constraint of lunate motion.

Craigie and Stanley attempted to reconcile the row versus column debate by examining scaphoid motion during wrist radial-ulnar deviation. They observed varying degrees of scaphoid flexion as the wrist radial deviated. In some wrists, there was substantial scaphoid flexion, indicating a “column-type” wrist, while in the others, the amount of scaphoid flexion was reduced [23]. This brings us to the question: why do these differences exist?

Previous work has shown a link between scaphoid motion and wrist laxity during wrist RUD [24], [25]. In these investigations, wrist laxity is defined by external measures of wrist flexibility; however, joint laxity does not have a single, unambiguous definition [26]. Joint

laxity is often associated with changes in ligament properties, as it is thought that “looser” ligaments allow for a larger range of motion at the wrist, while stiffer ligaments act to constrain carpal bone motion. To the best of our knowledge, ligament properties have not been directly linked to increasing range of motion at the wrist, so it is possible that other factors, such as carpal bone shape, could be involved.

In summary, a number of theories have been developed to explain carpal kinematics. Over time, it has been accepted the carpus acts neither as a series of rows or columns, and instead, normal carpal kinematics varies among individuals, resulting in variation in wrist range of motion and carpal bone motion patterns. Thus, one theory of carpal bone motion may not be sufficient for all individuals, as there are subject-specific factors leading to variation in bone motion. While this variation has been extensively examined on the radial side of the wrist, further research is required to understand the causes of this variation. Additionally, changes in carpal bone motion on the ulnar side of the wrist have yet to be investigated.

1.4 Measuring Carpal Bone Motion

Explaining carpal bone motion is an ongoing endeavour, with improvements in technology allowing for increasingly detailed and accurate measurement of carpal bone motion.

1.4.1 Static X-ray

Early theories of carpal kinematics were developed using static x-ray images. While x-ray imaging is inexpensive and can be used both *in vivo* and *ex vivo*, analysis is limited to static, two-dimensional images. This makes it difficult to understand how the carpal bones are moving, as the bones are often occluded. For example, studies that used static x-ray to investigate variability on scaphoid motion concluded that the scaphoid shortened more in some subjects than others during wrist RUD, but were unable to definitively state that what the observed shortening meant in terms of three-dimensional scaphoid motion [23], [24].

1.4.2 Optical Motion Tracking

Optical motion tracking uses exteriorly mounted markers to track motion. It has been successfully used *in vivo* to track global wrist motion [27], [28], but to accurately track the position of individual carpal bones, pins must be inserted into the bones to create an external visual signal. Using this method to track individual carpal bone motion is limited to *ex vivo* studies. Due to the close proximity of the carpal bones, it is often not possible to track all eight carpal bones during a single trial, as the optical markers may block each other's paths or interfere with wrist motion. For example, Patterson et al. postulated that marker interference limited wrist range of motion while tracking the carpal bones during simulated wrist motion trials [25]. Additionally, inserting pins into the carpal bones has the potential to disrupt the joint capsule, which could impact carpal bone kinematics.

1.4.3 Computed Tomography (CT)

CT scans of the wrist can be collected for both *in vivo* and *ex vivo* investigations. Traditional CT is limited to static postures of the wrist, so motion of the bones must be interpolated between positions. It is often assumed that the carpal bones move in a smooth arc between positions. Although this has the potential to introduce error in the reported carpal bone trajectories, evidence suggests a low hysteresis effect on carpal bone motion [29]. Unlike optical motion tracking, this method does not require any disruption to the joint capsule, and the entire carpus can be examined in each trial. Following segmentation and bone registration, carpal bone position measured from CT images is reported to be accurate to less than 1 mm of translational error and less than 2° of rotational error for all carpal bones [30], leading CT imaging to be considered the “gold standard” for reporting carpal bone motion.

1.4.4 Biplanar Videoradiography (BVR)

Biplanar videoradiography uses two high-speed x-ray sources to recreate dynamic, 3-dimensional motions at up to 1000 frames per second, and is suitable for use in both *in vivo* and *ex vivo*

subjects. Despite the appeal, this relatively new imaging methodology is difficult to apply to the wrist, as occlusion makes it difficult to track individual carpal bones. An initial study suggests that biplanar videoradiography has the potential to track global wrist position with similar or greater accuracy to optical motion capture [31], but to the best of our knowledge, this methodology has yet to be validated for tracking of carpal bones.

1.5 Summary and Objectives

The wrist is a highly complex joint which is essential for the performance of many activities of daily living. Although attempts have been made to understand how the carpal bones move within a healthy wrist, we have been left with many theories that cannot fully explain the spectrum of carpal bone motion that exists across the healthy population. Between individuals, there is known variation in ligament properties, carpal bone shape, and carpal bone size, which adds another layer of complexity when investigating carpal bone motion patterns.

Understanding the causes and ramifications of variation in carpal bone motion is a step towards developing a more robust biomechanical model of the wrist, which is able to consider subject-specific differences in carpal bone motion. The majority of research into variation in carpal bone motion has focused on the radial side of the wrist, in part due to the high prevalence of scapholunate ligament tears. To the best of our knowledge, variation in carpal bone motion has not yet been investigated on the ulnar side of the wrist. Understanding carpal kinematics in a healthy population is the first step towards improving biomechanical wrist models, understanding how pathology develops, developing new surgical techniques, and ultimately improving patient outcomes. With improvements in imaging technology, we now are able to move away from more generalized models and investigate the intricacies of carpal kinematics.

To advance our understanding of how the healthy wrist functions, we performed two studies to investigate natural variability in carpal bone motion using a CT database of 3D carpal bone postures. The goal of the first study was to develop our understanding

of how the triquetrum and lunate move in a healthy wrist during a variety of functional tasks. The primary objective was to determine whether the triquetrum moves together with the lunate as proposed by Linscheid et al. [15] and Lichtman [16], or whether it moves independently of the remainder of the proximal row as proposed by Sandow et al. [22]. As a secondary objective, we examined how the motion of the triquetrum changes with wrist flexibility. The aim of our second study was to investigate the effect of carpal bone shape on variation in carpal kinematics. The objective of this study was to determine whether shape of the scaphoid affected wrist range of motion. Together, these investigations help us to understand the causes and effects of variation in normal carpal kinematics, laying the foundation for future investigations into differential responses to injury and treatment, with the potential to inform targeted, patient-specific interventions.

Chapter 2

The Intercalated Segment: Does the Triquetrum Move in Synchrony with the Lunate?

2.1 Introduction

The most prominent theory of carpal instability is the “the balanced lunate” concept – proposed by Garcia-Elias [32]. This theory states that in the healthy wrist, the triquetrum and the scaphoid place opposing moments on the lunate [6]. If the scapholunate interosseous ligament (SLIL) and critical supporting ligaments are torn, the scaphoid no longer applies a flexion moment to the lunate through the SLIL. The triquetrum then pulls the lunate into extension via the lunotriquetral interosseous ligament (LTIL). This causes dorsal intercalated instability (DISI), which can lead to pain, reduced range of motion, and ultimately to degenerative arthritis [7]. If the LTIL and critical supporting ligaments are torn, the scaphoid pulls the lunate into flexion via the SLIL causing volar intercalated segment instability (VISI). While VISI can invoke symptoms, they seem to be less severe and less common than those associated with DISI [33].

In this model, a key assumption in the pathomechanics of DISI is the triquetrum driving the lunate into extension via the LTIL. Thus, investigating the role of the triquetrum in the intact wrist is a critical step toward understanding how carpal instability develops. Linscheid et al. lent support to the “balanced lunate” concept by suggesting that, in the healthy wrist, the lunate and triquetrum move together as a unit, which he called an

“intercalated segment” [15]. Based on this assumption, LT arthrodesis has been recommended for chronic LT instability [5], [34], [35], but results have been inconsistent [36], [37]. Although the “intercalated segment” theory of triquetral motion is thoroughly embedded in the literature, to the best of our knowledge it has yet to be studied.

Subject-specific variation in carpal bone motion may impact the triquetrum’s ability to drive the lunate into extension. For example, wrist laxity has been found to influence carpal bone motion. A spectrum of normal carpal kinematics has been observed in healthy wrists [23], and correlations have been found between the motion of the scaphoid and wrist laxity [24], [25]. Thus, it is probable that changes in wrist laxity can affect the triquetrum’s ability to drive the lunate into extension. Due to the prevalence of scapholunate lunate ligament injuries, the motion of the scaphoid and lunate has been studied extensively [38]–[43] while less work has been done to understand how the triquetrum moves [44], [45].

Understanding the subject-specific factors governing carpal mechanics in the intact wrist can help explain differential responses to injury and treatments, and potentially inform targeted, patient-specific interventions that restore native function. The purpose of this study was to directly test Linscheid’s intercalated segment theory *in vivo* in healthy wrists, and to better understand the influence of generalized carpal laxity on triquetral kinematics. We hypothesized that 1) the triquetrum and lunate would move as a rigid body during functional wrist motions, including radial-ulnar deviation (RUD), flexion-extension (FE) and functional movements, and 2) there would be increased rotation of the triquetrum with increased wrist laxity during all wrist motions.

2.2 Methods/Materials

2.2.1 Subject Selection and Data Collection

This study further analyzed data from 10 volunteers who participated in our previous investigation on the influence of carpal laxity on scaphoid and lunate motion [25]. After REB approval [46] and informed consent, 17 right-handed volunteers were screened for wrist

laxity and wrist pathologies. From these 17 volunteers, 10 participants (six females, four males; average age 32 years, range 19-52 years) with no current or prior wrist pathologies were selected for further analysis. Participants were selected so that a wide spectrum of wrist laxity was represented in the participant population. This was done to limit the radiation dosage and processing time while still sampling a wide range of laxity. We used a manual goniometer to measure wrist range of motion based on palpated bony landmarks, taking both active and passive measurements. Based on findings that carpal ligaments are the most strained in extreme flexion and extension [47], we used passive FE range of motion from the goniometer measurements as a surrogate measure for wrist laxity, similar to previous work [24]. The measured passive FE range of motion used in our analysis was the average of three measurements taken for each subject. Across ten subjects, the passive FE range of motion varied from 151° to 229° .

We performed computed tomography (CT) on the subjects' right wrists in seven targeted positions: neutral, maximum flexion, maximum extension, maximum radial deviation, maximum ulnar deviation, targeted radial deviation (20°), and targeted ulnar deviation (20°). A plexiglass and polycarbonate jig was used to position the subjects and a manual goniometer was used to confirm each position by placing the goniometer on the dorsal side of the wrist (dorsal-volar technique) [48]. We also performed CT during a hammering task by giving the subject a dowel to hold, which was positioned against the jig to simulate a hammering motion, similar to previous work (Figure 2.1) [49]. Images were taken in three equally spaced positions along a 90° arc, targeting a smooth arc from radial extension to ulnar flexion. All images were taken using a GE Bright-speed CT scanner (GE Medical, Milwaukee, WI) at 80 kV, with a slice thickness of 0.625 mm. The in-plane resolution was 0.2×0.2 mm in the neutral position and 0.3×0.3 mm in all other positions.

2.2.2 Data Processing and Kinematic Analysis

We segmented the images from the CT scans using Mimics 17.0 (Materialise, Leuven, Belgium), and generated surface files for the radius, ulna, carpal bones, and metacarpals.

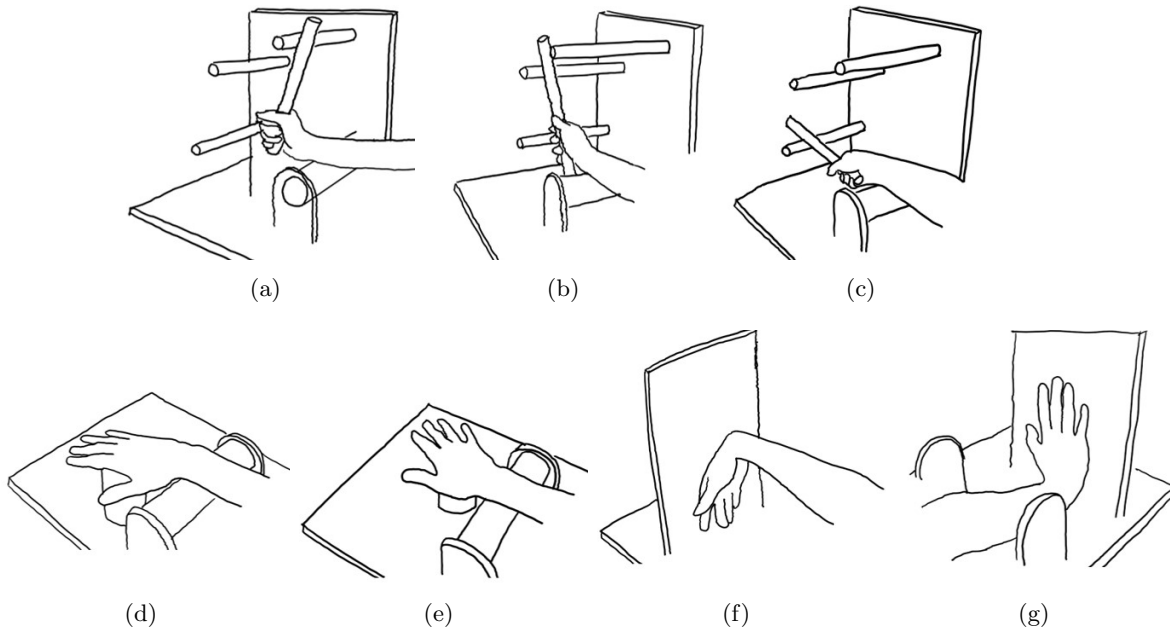


Figure 2.1: Wrist positioning during CT scanning: (a) Hammer 1, (b) Hammer 2, (c) Hammer 3, (d) radial deviation, (e) ulnar deviation, (f) maximum flexion, and (g) maximum extension.

For each bone in each position, we calculated the centroid location (in mm) and the inertial axes using MATLAB R2018b (Mathworks, Natick, MA) [50]. Kinematic transforms were used to move each bone from neutral to the other targeted positions. For fully enclosed bone surfaces (eg: the carpal bones), the transforms were calculated using inertial registration, and for cropped bones such as the radius and ulna, a surface-matching algorithm was used in Geomagic Wrap (Raindrop Geomagic, Research Triangle Park, NC) [51], [52]. Bone position was expressed in a radius-based anatomical coordinate system (ACS) to compare carpal bone positions in different postures (Figure 2.2) [53].

We then computed the rotation axes (helical axes of motion) of the lunate and triquetrum relative to the radius. This allowed us to compare the amount the bones rotated, as well as the location and orientation of the axis about which they rotated. For wrist radial deviation, ulnar deviation, flexion and extension motions, the rotation axis was computed between clinical neutral and the selected position. We excluded any rotation axes that demonstrated less than 5° of carpal bone rotation.

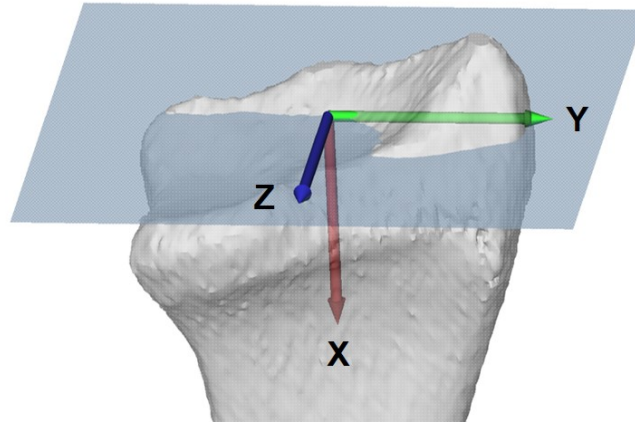


Figure 2.2: Volar view of the right radius, showing the radius-based anatomical coordinate system which consists of the pronation-supination (X), flexion-extension (Y) and radial-ulnar deviation (Z) axes with the transverse (YZ) plane overlaid

To determine whether the lunate and triquetrum moved as a rigid body, we analysed the triquetrum-radius and lunate-radius rotation axes. If the triquetrum and lunate were moving as a single rigid body, their rotation axes would be identical. We projected these axes into the transverse FE/RUD (YZ) plane (Figure 2.2) and then computed the angle between the triquetrum-radius rotation axis and the lunate-radius rotation axis for each subject during each wrist movement. The average angle between these rotation axes and the standard deviation was computed for each movement. We used G*Power 3.1.9 (Dusseldorf University, Dusseldorf, Germany) to perform a retrospective power analysis on the data. A 1-population t-test with a hypothesized mean of zero was used to determine whether paired rotation axes had the same orientation. With sample size of 10 subjects, the statistical power of the sample size was greater than 85% for all angles examined.

Additionally, we looked for relative motion between the proximal carpal bones, as this would be minimal between bones that were moving synchronously. We computed the lunate-triquetrum rotation axes, identified the maximum amount of rotation across all subjects and motions, and used Tukey's honestly significant difference (HSD) test to determine whether the amount of relative rotation was different between pairs of wrist motions ($p < 0.05$). To control for the effect of variation in the amount of wrist rotation, for each participant,

we also computed the rotation between the lunate and triquetrum as a percentage of their total wrist rotation.

To determine whether triquetral motion was influenced by wrist laxity, we looked at the motion of the triquetrum during wrist motion from 20° of radial deviation to 20° of ulnar deviation. This targeted range of motion ensures that differences in carpal bone motion are not simply due to an increased range of wrist motion. We compared the amount of rotation, location (scaled to wrist size), and orientation in the transverse (YZ) plane of the triquetrum-radius rotation axis to the passive FE range of motion. To compare the location of the rotation axes among subjects, we scaled the axis location by capitate length to account for variation in wrist size [54]. Linear regression of rotation axis location as a function of passive range of motion was performed and the coefficient of determination (R^2) was computed. We used an F-test to determine whether the slope of the regression was statistically different from zero ($p < 0.05$).

2.3 Results

2.3.1 Wrist Positioning

During the neutral scan, we targeted a wrist position of 0° FE, 0° RUD; however, the average wrist position was $9 \pm 7^\circ$ F, $1 \pm 6^\circ$ UD, indicating that the wrist was slightly flexed. During the hammering task, the average wrist positions were: Hammer 1 ($47 \pm 12^\circ$ E, $3 \pm 8^\circ$ RD), Hammer 2 ($25 \pm 11^\circ$ E, $27 \pm 8^\circ$ UD), and Hammer 3 ($12 \pm 12^\circ$ F, $35 \pm 8^\circ$ UD).

2.3.2 Global Carpal Bone Motion

In contrast to our hypothesis, the triquetrum and lunate did not always move as a rigid body throughout wrist motion. From Hammer 1 to 2, the lunate-radius rotation axis and the triquetrum-radius rotation axis had dissimilar orientations and locations (Table 2.1), and the orientation and location of the rotation axes were variable across subjects (Figure 2.3). However, the triquetrum and lunate moved together through the second step of the hammering

task (Hammer 2 to 3). Here, the lunate-radius and triquetrum-radius rotation axes became closely aligned (Figure 2.3), with the lowest average angle between these two axes observed in any motion studied (Table 2.1). A low average angle (less than 20°) between the triquetrum-radius and lunate-radius rotation axes was also observed in all motions except radial deviation and Hammer 1 to 2.

Table 2.1: Average angle (in degrees) between the triquetrum-radius or scaphoid radius helical axis and the lunate-radius helical axis, projected into the FE-RUD plane (Figure 2.2). Bolded values indicate an average angle between the axes below 20° , which suggests that the bones are moving together.

Motion	Hammer 1 to 2	Hammer 2 to 3	20° Radial Deviation*	20° Ulnar Deviation	Maximum Radial Deviation*	Maximum Ulnar Deviation	Maximum Flexion	Maximum Extension
Angle Between Rotation Axes	38.5 ± 12.2	5.6 ± 4.2	43.1 ± 25.4	16.6 ± 13.3	41.0 ± 18.1	11.0 ± 6.2	7.1 ± 6.9	5.9 ± 4.6

*indicates that subjects were excluded from this analysis due to carpal bone rotation less than 5° (2 subjects in mid-range radial deviation and 3 subjects in maximal radial deviation)

2.3.3 Intercarpal Rotation

The minimal measured rotation ($< 9.5^\circ$) between the lunate and the triquetrum occurred as the wrist ulnar-deviated (Figure 2.4), while rotation between the scaphoid and lunate was minimal ($< 5^\circ$) in radial deviation. Across all motions and subjects, we observed a maximum of 23° of rotation between the lunate and triquetrum.

2.3.4 Wrist Laxity

We did not find a correlation ($p = 0.55$) between the amount of rotation of the triquetrum and passive FE range of motion as the wrist moved from 20° of radial deviation to 20° of ulnar deviation. During this motion, the triquetrum primarily radial-ulnar deviated ($68 \pm 11\%$ RUD, $28 \pm 12\%$ FE, $5 \pm 7\%$ PS), while the lunate ($29 \pm 13\%$ RUD, $67 \pm 14\%$ FE, $3 \pm 4\%$ PS) primarily flexed and extended. However, as the passive FE range of motion increased, there was a tendency for a greater component of flexion-extension in the movement of the triquetrum ($p = 0.066$) (Figure 2.5). We also observed a relationship between the passive

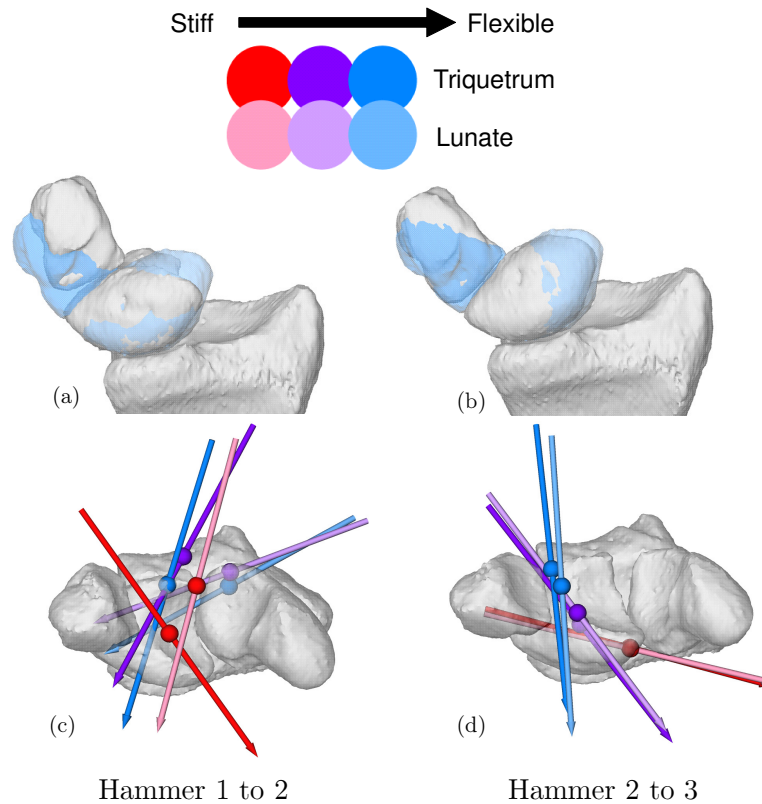


Figure 2.3: Image of the lunate - radius (light colours) helical axes compared to the triquetrum-radius helical axes (dark colours) for 3 representative subjects with various degrees of wrist flexibility. The axes are superimposed on the bones of a representative subject, with the carpal bone motion shown in (a, b). The left images (a, b) show the axes and carpal bone motion during Hammer 1 to 2. The right images (b, d) show the axes during Hammer 2 to 3. In (d), the light and dark axes are aligned, showing that the lunate and triquetrum are moving as a rigid body.

FE range of motion and the location of the triquetrum-radius rotation axis. As the wrist moved from Hammer 2 to 3, the triquetrum-radius and lunate-radius rotation axis moved distally with increased passive FE range of motion ($p = 0.0004$, $R^2 = 0.85$), so that the rotation axes shifted from piercing the lunate to piercing the proximal pole of the hamate (Figure 2.6). During this movement, there was no correlation between passive FE range of motion and wrist position ($p > 0.5$, $R^2 < 0.06$). Thus, changes in carpal motion associated with increased wrist laxity were not due to an increased range of motion at the wrist.

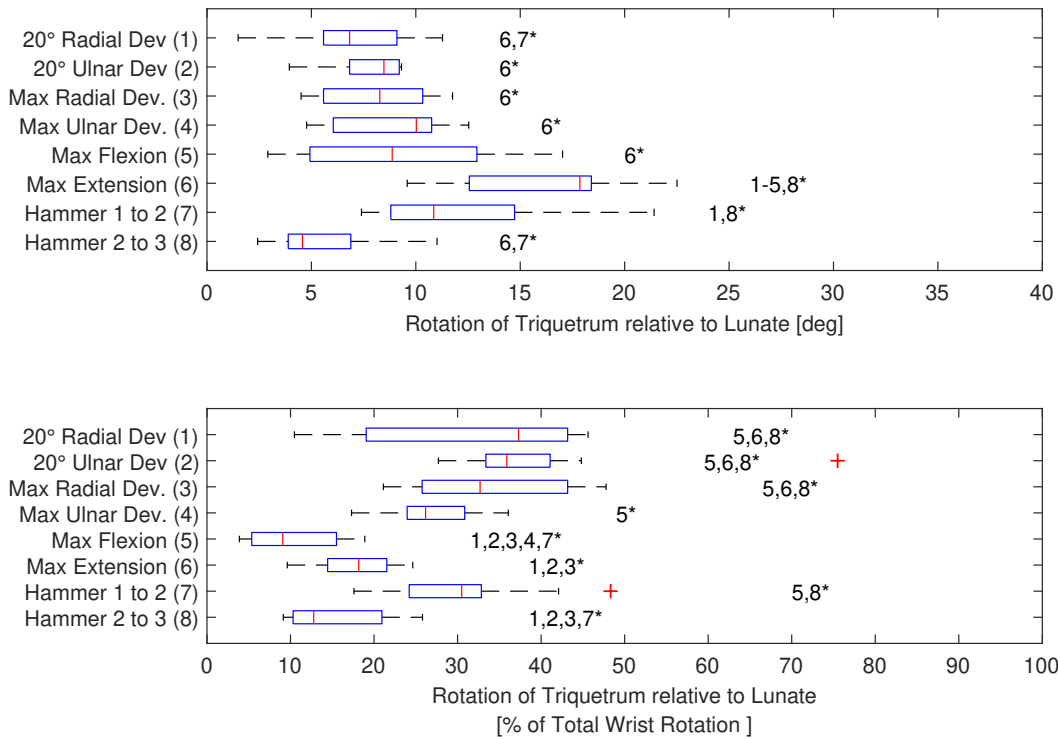


Figure 2.4: Comparison of the relative rotation (ϕ) between the lunate and triquetrum for a series of wrist motions, found by computing the helical axis of rotation between the two bones. Asterisks are used to indicate a significant difference ($p < 0.05$) between two motions.

2.4 Discussion

We investigated Linscheid’s idea that the triquetrum and lunate function as an intercalated segment – moving together. We found that the lunate and triquetrum moved very nearly as a rigid body as the wrist moved from Hammer 2 to Hammer 3 and from neutral to ulnar deviation but did not move as a rigid body from radial deviation to functional neutral. Wrist laxity influenced the orientation and location of the triquetrum-radius rotation axis during mid-range radial-ulnar deviation.

During wrist radial-ulnar deviation, we observed that the triquetrum tended to primarily radial-ulnar deviate. This is inconsistent with several previous studies, which suggested that the bones in the proximal carpal row flex and extend during wrist radial ulnar deviation [44],

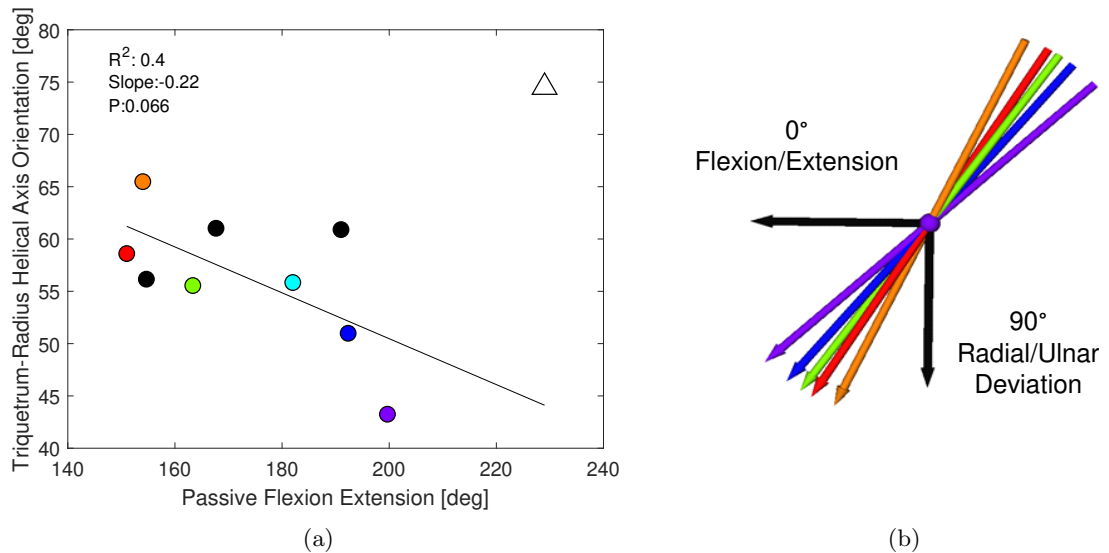


Figure 2.5: (a) As passive flexion-extension range of motion increased across subjects, the triquetrum underwent more flexion-extension during wrist radial-ular deviation. Orientation greater than 45° indicates that the triquetrum is primarily radial-ular deviating, while orientation below 45° would indicate that the triquetrum is primarily flexing and extending. An outlier was excluded due to low carpal bone rotations. (b) Visualization of the helical axes, where colours are used to identify subjects. The origin of the helical axes has been shifted to $[0,0,0]$ to make the change in orientation more visible.

[55]–[57]. While it is well established that the scaphoid and lunate primarily flex and extend [3], [39] it is an important distinction that the triquetrum primarily radial-ular deviates during wrist radial-ular deviation. This further emphasizes that the triquetrum moves distinctly from the lunate.

Our results also show that there was variation in the carpal bone motion among subjects, with a greater component of flexion-extension in the motion of the triquetrum in participants with more lax wrists compared to those with stiffer wrists. From Hammer 2 to Hammer 3, the triquetrum-radius and lunate radius-rotation axes were located more distal in lax wrists compared to stiffer wrists, such that the axis location changes from piercing the lunate to piercing the hamate. We postulate that this indicates increased interaction between the triquetrum and hamate, which has been hypothesized to provide “rotational control” over the proximal carpal row [21].

Given the “balanced lunate” theory of Garcia Elias [6], it is possible these differences

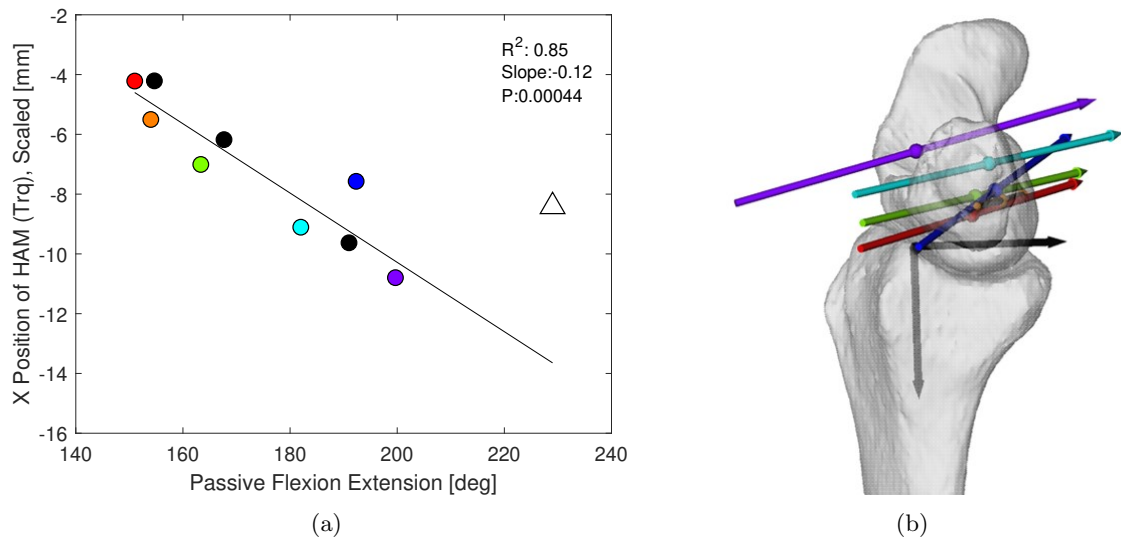


Figure 2.6: (a) During Hammer 2 to 3, in subjects with laxer wrists the triquetrum-radius helical axis shifts upwards. (b) Visualization of the helical axes. For this analysis, the locations of the helical axes were scaled by the length (proximal-distal axis) of the capitate to account for differences in wrist size. An outlier was excluded due to low carpal bone rotations, consistent with previous work [25].

in triquetral motion associated with wrist laxity may influence the triquetrum's ability to extend the lunate. However, this hypothesis cannot be answered with the methods presented here. If true, it would have important implications for ligament reconstructions. For example, following ligament injury, reconstructions that replace the ligament with donor tendons or rely on joint arthrodesis may need to consider the effects of the reconstruction based on a patient's native laxity. Variation in the native amount of relative motion between the lunate and triquetrum may also provide some insights into the variable results seen following lunotriquetral arthrodesis [36].

We observed a maximum of 23° of intercarpal rotation between the lunate and triquetrum, which occurred as the wrist moved from neutral to maximum extension. This is slightly more than the 18° observed in previous work by Ruby et. al. [56], and considerably more than the 4° Weber observed [21]. Unlike our work, these studies were limited to *ex vivo* analysis using biplanar x-ray, and did not include functional tasks. However, our results agree with more recent work by Moritomo et al., who observed up to 21° of rotation between

the lunate and triquetrum during a dart throw [17]. Unlike previous work, we considered extreme wrist positions, which may help account for discrepancies in the measured rotation.

Recent work has used CT to investigate carpal bone motion, but the primary focus been the scaphoid and lunate. Investigation of triquetral motion using CT to date has often focussed on its interaction with the hamate [58], [59]. Crisco et al. found that the flexion of the triquetrum was not significantly different from that of the lunate [60] during wrist flexion. Moritomo et. al. examined motion of the triquetrum relative to the capitate in vivo using magnetic resonance imaging (MRI) during wrist FE, RUD, and along a dart thrower's path [17]. Our work used CT to examine the motion of the triquetrum relative to the radius during wrist RUD, extreme FE, and during a hammering task, providing new information about the intricacies of its movement. To build on the current understanding of carpal bone kinematics, we used wrist laxity to help us identify and explain changes in wrist motion across subjects.

The primary limitation of this study is that carpal bone motion was inferred from pairs of static postures; thus, we assumed that the rotation axes had a consistent orientation and location when moving between neutral and the targeted poses. In addition, our hammering task was limited to three poses, unlike the 5-position hammering task used a similar study [49]. In the intermediate position of our hammering task, we found that our subjects' wrists ulnar deviated more than expected, with an average wrist position of $25 \pm 11^\circ$ E, $27 \pm 8^\circ$ UD compared to $36 \pm 8^\circ$ E, $14 \pm 10^\circ$ UD in a similar task [49].

We attempted to control wrist position to 20° of radial deviation and 20° of ulnar deviation, but two of the subjects could not reach the target 20° of radial deviation, reaching only 9° and 15° degrees of radial deviation. While we took CT scans in a variety of poses, we did not collect mid-range flexion or extension poses that may have served as a better point of comparison to the amount of flexion or extension observed during the hammering task. As expected, for maximum poses, there were correlations between wrist position and subject laxity.

Additionally, we only collected data from 10 subjects. Our most hypermobile subject

had extremely low carpal bone rotations, which led them to be excluded from the rotation axis position and orientation analysis since this causes the rotation axis to become highly sensitive to noise [25]. To deepen our understanding of how the carpal bones move across the spectrum of healthy subjects, it would be useful to collect data from more participants, particularly those on the higher end of the laxity spectrum.

Our findings can be applied to help us understand how the entire proximal row functions. In contrast to earlier theories, Sandow acknowledged that the lunate and triquetrum move as independent structures, which agrees with our findings [22]. Sandow suggested that the wrist functions as a two gear, four bar linkage, where the triquetrum's main role is as an ulnar translation restraint, but it also controls lunate flexion [22]. Our results augment current carpal models of carpal kinematics by highlighting the natural variability in carpal bone motion on a subject specific level. Subject specific factors, such as those related to laxity, may be important for disease progression as well as reconstructive approaches.

In summary, we have shown that the triquetrum and lunate did not always move in synchrony throughout the range of wrist motions investigated, with more synchronous motion occurring in flexion and the later stages of our hammering task. We also found that the motion of the triquetrum varies with wrist laxity. More work is needed to determine whether changes in the motion of the triquetrum influence its ability to extend the lunate, and how this may influence the development of volar or dorsal intercalated segment instability.

Chapter 3

Influence of Scaphoid Morphology on Wrist Range of Motion

3.1 Introduction

Movement at the human wrist is essential for performing many activities of daily living [61]. It has been shown that the majority of these activities can be performed with a functional range of motion, consisting of 40° of flexion, 40° of extension, and 40° of combined radial and ulnar deviation [62]. From an evolutionary perspective, it has been theorized that the functional wrist range of motion in humans compared to other primates may have provided advantages by allowing for tool use. For example, the ability of the wrist to move through a large range of wrist motion while holding a blunt weapon increases the impact power that can be delivered [2].

Subject-specific variation in wrist range of motion has been previously attributed to variation in ligamentous laxity [24], [25]. Laxity is frequently used interchangeably with range of motion; however, exact definitions of laxity vary [26]. Laxity has been described as displacement of the joint when subjected to stress, or as a condition in which joints have a larger than normal range of motion. Often, ligamentous laxity is used to describe increased range of motion which is thought to occur as a result of reduced ligament stiffness. However, both ligament properties and bone shape [63] are important for facilitating carpal bone motion, so it is possible that bone shape may also play a role in determining wrist flexibility.

To date, investigations linking carpal bone shape to carpal kinematics have mainly

focussed on the lunate. Variation in lunate type (defined by the presence or absence of an articular facet for the hamate) has been linked to changes on motion of the lunate [64], and type II lunates (defined by the presence of an articular facet for the hamate) have been linked to increased prevalence of osteoarthritis at the base of the hamate [65]. However, to the best of our knowledge, the effects of shape variation in the carpal bones have yet to be investigated in the context of determining wrist range of motion.

Among the carpal bones, the scaphoid has a unique role in that it bridges the proximal and distal carpal rows, and has been found to transmit over 50% of the force through the carpus [66]. Thus, it has been proposed that the scaphoid acts as a supporting column to the carpus [21], [22], playing a crucial role in joint mechanics. During wrist flexion-extension (FE) and radial-ulnar deviation (RUD), the scaphoid tends to primarily flex and extend. In previous work, variation in scaphoid motion has been observed between individuals [23]–[25], [45]. This has been attributed to changes in ligamentous laxity [24], [25], [67]; however, the role of scaphoid morphology in scaphoid kinematics has not been considered.

Statistical shape modelling is a tool that uses principal component analysis to visualize and quantify variability in bone shape across a given population. Previous work with statistical shape modelling has linked bone shape to joint mechanics in other joints, such as the knee [68]. To date, statistical shape modelling has been used to describe the shape variation in the scaphoid [69], but to the best of our knowledge, this variation has not yet been linked to carpal bone kinematics.

Understanding the role of bone shape in determining wrist range of motion can help us to identify the causes of subject-specific variation in carpal bone motion, further developing our understanding of how the human wrist functions. Our primary goal was to determine how scaphoid morphology affects wrist laxity and carpal bone kinematics. We expected that variation in scaphoid shape would restrict scaphoid movement at the radiocarpal joint, decreasing the wrist range of motion (ROM). As a secondary objective, we looked for a connection between scaphoid shape and scaphoid posture in the neutral wrist [25], and determined whether scaphoid posture impacts wrist range of motion.

3.2 Methods/Materials

3.2.1 Subject Selection and Data Collection

This work further analyzed data from 10 volunteers, who participated in a previous investigation of the influence of wrist flexibility on the motion of the proximal carpal row [25]. From a pool of 17 volunteers, 10 volunteers with no current or prior wrist pathologies were chosen that spanned a range of wrist laxity, measured as passive flexion-extension wrist ROM. Across the ten selected subjects, the passive FE range of motion varied from 151° to 229°. A manual goniometer placed on the dorsal side of the wrist (dorsal-volar technique) was used to measure wrist ROM [48]. Passive measurements were taken for wrist flexion, extension, radial deviation, and ulnar deviation, where subjects were instructed to apply force to their own hand to increase the angle between the forearm and the hand until they felt discomfort. Three measurements were taken in each position, and then averaged to give a representative measurement for each subject.

The subjects' right wrists were imaged in neutral, maximum flexion, maximum extension poses, maximum radial deviation, and maximum ulnar deviation poses. For the maximum poses, the subjects were instructed to hold their wrist against a surface, increasing the angle between the forearm and the hand until they felt slight discomfort. Images were taken using a GE Bright-speed CT scanner (GE Medical, Milwaukee, WI) at 80 kV, with a slice thickness of 0.625 mm.

3.2.2 Image Processing

The images were segmented to generate surface meshes for the radius, ulna, carpal bones and metacarpals using Mimics 17.0 (Materialise, Leuven, Belgium). We calculated the centroid location and inertial axes of each bone in each position using MATLAB R2018b (Mathworks, Natick, MA) [50]. Kinematic transforms were then generated to describe the motion of each bone from the neutral position to each of the other positions investigated. For enclosed bones, such as the carpal bones, inertial registration was used to calculate

the transforms, while for cropped bones such as the radius and ulna, a surface-matching algorithm in Geomagic Wrap (Raindrop Geomagic, Research Triangle Park, NC) [51], [52]. These methods are reported to be accurate to less than 2° of rotation and 1 mm of translation for all carpal bones [30].

3.2.3 Principal Component Analysis

A statistical shape model of the scaphoid was generated to investigate variation in scaphoid morphology. Fourteen scaphoid surfaces from a publically available database [70] were added to the 10 surfaces collected above, for a total of 24 scaphoid surface meshes. Each bone was then registered to its own anatomical coordinate system, to ensure that bone alignment would not be included the statistical shape model. We used the Coherent Point Drift algorithm [71] to establish node correspondence between surfaces, with the reference mesh selected as the mesh with the mean surface area. A Procrustes analysis in MATLAB R2018b (Mathworks, Natick, MA) was used to scale and further align the scaphoids, by minimizing the sum of squared distances between nodes. Then, we applied principal component (PC) analysis to all 24 scaphoid meshes to create a statistical shape model independent of scaling and alignment. Using previously established methods, we computed the number of stable modes to validate our sample size [72]. With 24 subjects, we had seven stable modes of scaphoid shape variation.

To investigate the impact of scaphoid shape on wrist range of motion, we used linear regressions to compare the principal components of scaphoid shape to the wrist ROM measurements, and computed the correlation coefficients (R^2). We used F-tests to determine whether the slopes of the regressions were statically different from zero ($p < 0.05$). To help alleviate the effects a low sample size, we also performed leave one out regression to further characterize the statistical strength of any correlations between the principal components of scaphoid shape and wrist range of motion measurements.

3.2.4 Bone Position and Contact Region Analysis

To explore the sources of ROM variation associated with changes in bone morphology, we examined the contact region between the scaphoid and radius, as well as between the scaphoid and capitate in maximum flexion, maximum extension, and neutral. For this analysis, we estimated the cartilage contact area, as the cartilage was not imaged directly. In accordance with previous work, we estimated an articular cartilage thickness of 0.9 mm on each bone surface [59]. Thus, a pair of bones would be in contact if the distance between adjacent bone surfaces was less than or equal to 1.8 mm. Iso-contour distances between each pair of bones were calculated using previously established methods [73], and the region in which the bone surfaces were within 1.8 mm of each other in was determined in each position.

Then, we computed the rotation axes between pairs of adjacent carpal bones to look for variation in carpal kinematics. We compared the amount of rotation between the scaphoid and radius to the amount of rotation between the scaphoid and capitate during wrist flexion and extension. Previous work has shown that scaphoid posture, defined as the neutral scaphoid flexion angle, is variable between subjects [25], so we suspected that this may impact the reported amounts of scaphoid rotation. We investigated the influence of scaphoid posture on variation in carpal bone motion by comparing the flexion angle of the scaphoid in clinical neutral (Figure 3.1) to scaphoid rotation and scaphoid shape.

3.3 Results

3.3.1 Principal Component Analysis

For our analysis, we chose to focus on the first five principal components of scaphoid shape, which cumulatively explained 65% of the shape variation. We found that the first principal component (PC1) was positively correlated with passive flexion ($R^2 = 0.67$, $p < 0.01$) and the second principal component (PC2) was negatively correlated with passive extension ($R^2 = 0.46$, $p < 0.05$) (Figure 3.2). There was no correlation between any of the

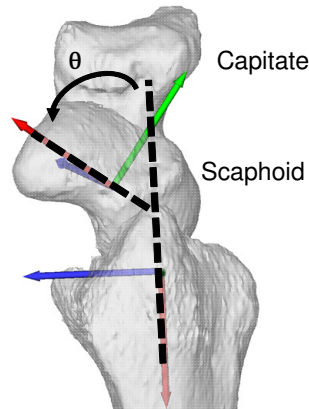


Figure 3.1: Scaphoid posture, measured by computing the angle between the principal inertial axes (red) of the radius and scaphoid while the wrist is in clinical neutral.

first five principal components and passive radial deviation. However, a correlation was observed between PC1 and passive ulnar deviation ($R^2 = 0.51$, $p < 0.05$). PC1 values altered the shape of the concave scaphoid facet, while high PC2 values elongated the distal tubercle of the scaphoid (Figure 3.3). From the leave one out analysis, all combinations showed evidence of a correlation between PC1 and passive flexion ($R^2 > 0.5$, $p < 0.03$), 9 of 10 combinations showed evidence of a correlation between PC2 and passive extension ($R^2 > 0.4$, $p < 0.05$), and 8 of 10 combinations showed evidence of a correlation between PC1 and passive ulnar deviation ($R^2 > 0.4$, $p < 0.05$).

3.3.2 Bone Position and Contact Region Analysis

In maximum flexion, we did not observe a correlation between rotation of the scaphoid relative to the radius and the rotation of the third metacarpal relative to the radius ($R^2 = 0.14$, $p = 0.3$), but did observe a positive correlation between the rotation of the capitate relative to the scaphoid and rotation of the third metacarpal relative to the radius ($R^2 = 0.55$, $p = 0.014$) (Figure 3.4 a,b). This suggests that variation in the subjects' range of motion in wrist flexion may be associated with increased relative motion between the capitate and scaphoid. We did not observe any differences in the size or location of the contact region between the scaphoid and radius in wrist flexion.

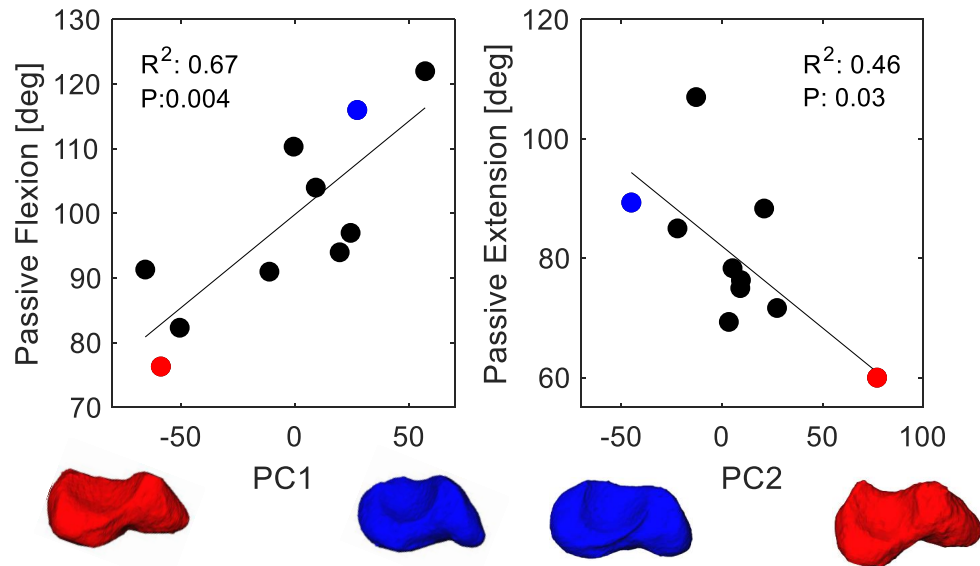


Figure 3.2: Principal components of scaphoid shape are correlated with subjects' passive flexion (left) and passive extension (right) range of motion. The scaphoids of representative subjects with low (red) and high (blue) ranges of motion are shown to illustrate shape features.

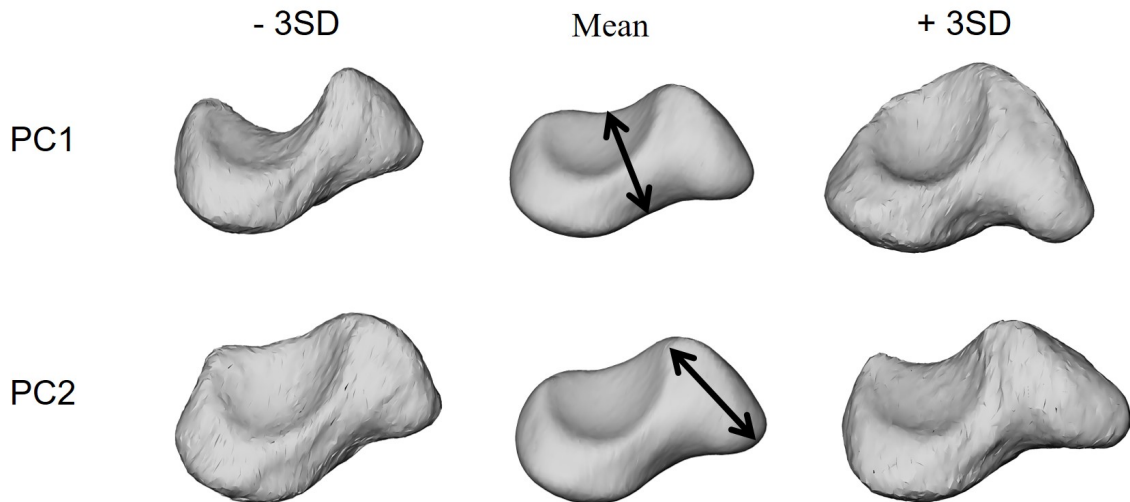
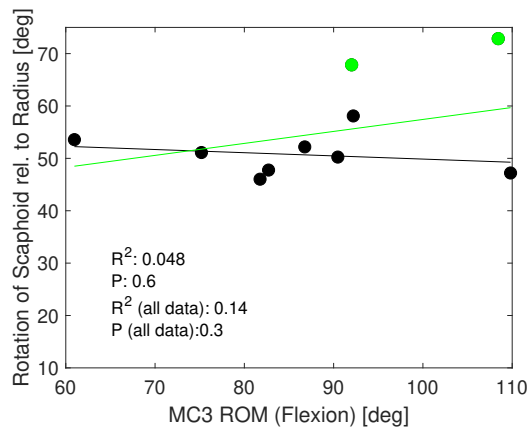
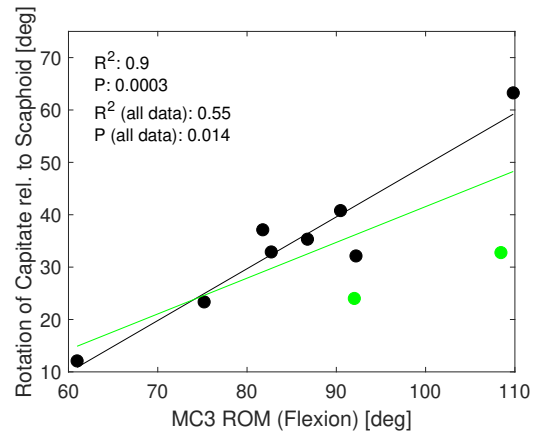


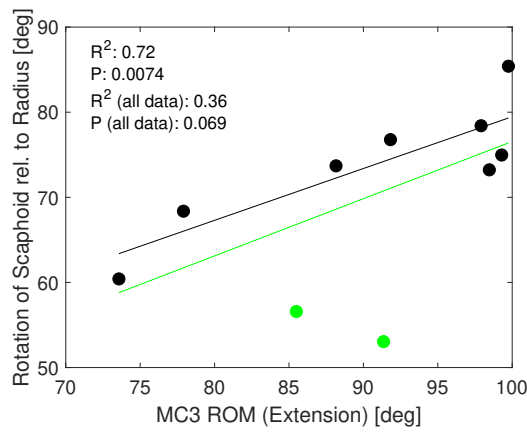
Figure 3.3: Simulated images to show the first two principle components of scaphoid shape. PC1 explained 30% of the shape variation, while PC2 explained 12%. PC1 changed the thickness of the waist of the scaphoid, altering the shape of the concave scaphoid facet. PC2 changed the length of the distal scaphoid tubercle.



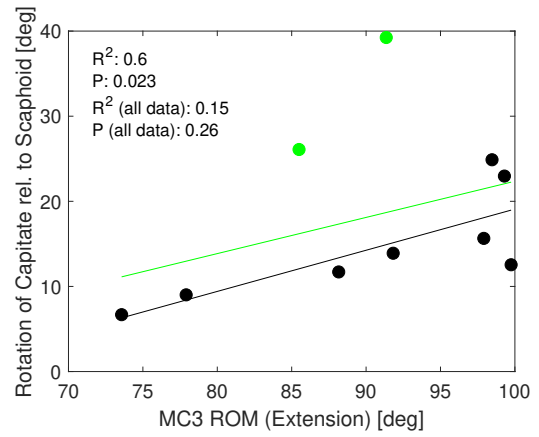
(a)



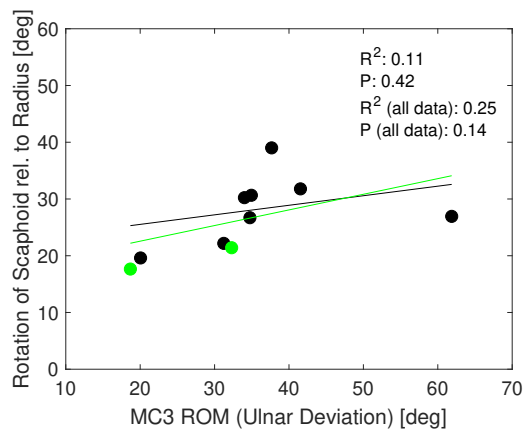
(b)



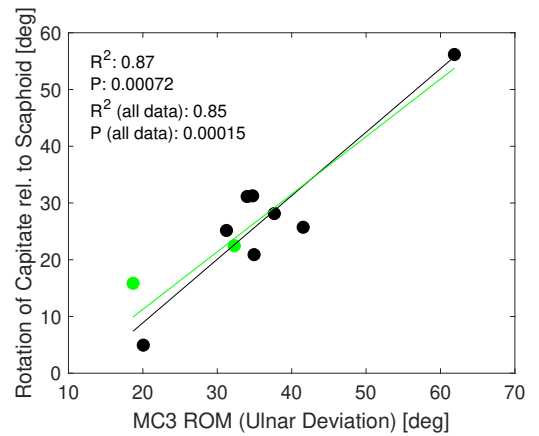
(c)



(d)



(e)



(f)

Figure 3.4: Rotation between the scaphoid and radius (a, c, e) or capitate (b, d, f) during wrist flexion and extension. The two subjects with the lowest scaphoid angle in neutral (least flexed scaphoids) are shown in green. The black regression line excludes these two subjects, while the green regression line includes all subjects

In maximum extension, we observed a correlation between rotation of the scaphoid relative to the radius and the rotation of the third metacarpal relative to the radius ($R^2 = 0.36$, $p = 0.069$), but did not observe a correlation between the rotation of the capitate relative to the scaphoid and rotation of the third metacarpal relative to the radius ($R^2 = 0.15$, $p = 0.26$) (Figure 3.4 c, d). No consistent differences were observed in the size or location of the scaphoid-radius or scaphoid-capitate contact areas.

We did not find evidence of a correlation between rotation of the scaphoid relative to the radius and rotation of the third metacarpal relative to the radius in maximal wrist ulnar deviation ($R^2 = 0.25$, $p = 0.14$). However, increased rotation between the scaphoid and capitate was correlated with a larger range of motion in ulnar deviation ($R^2 = 0.85$, $p < 0.01$).

3.3.3 Scaphoid Posture

In wrist flexion and extension, rotation of the scaphoid relative to the radius was correlated with neutral scaphoid posture (Figure 3.5). There was no correlation between the neutral scaphoid flexion angle and the first five principal components ($R^2 < 0.2$, $p > 0.2$), or between the neutral scaphoid flexion angle and passive flexion or extension range of motion ($R^2 < 0.001$, $p > 0.8$). During wrist extension in the two subjects with the lowest scaphoid flexion, we saw less rotation of the scaphoid relative to the radius, and more rotation of the capitate relative to the scaphoid (Figure 3.4).

3.4 Discussion

We used statistical shape modelling to investigate how scaphoid morphology influences wrist range of motion. The first and second principal components of scaphoid shape were correlated with wrist flexion and extension range of motion, respectively. Scaphoid posture was not correlated with wrist range of motion, but scaphoid posture did influence scaphoid kinematics as the wrist flexed and extended.

Although our contact region analysis was inconclusive, we have several theories as to

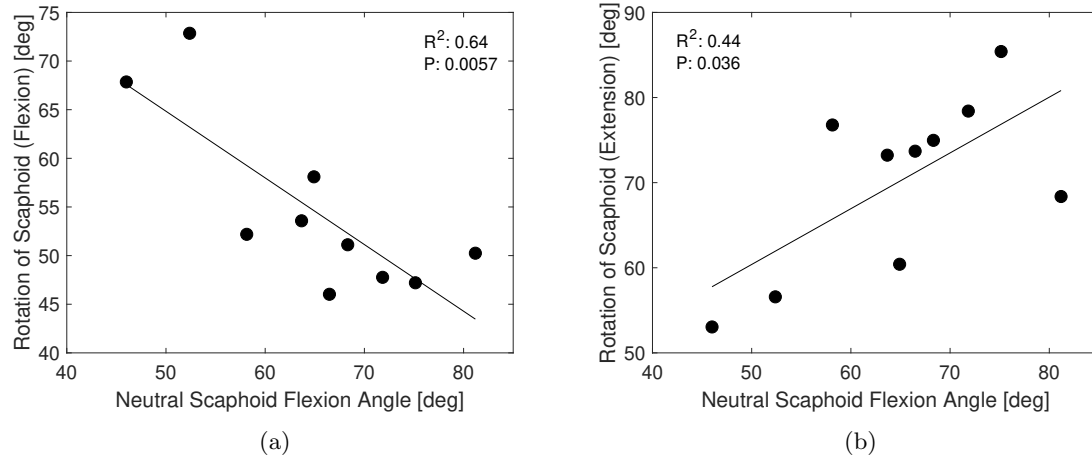


Figure 3.5: (a) During wrist flexion, rotation (flexion) of the scaphoid decreased in scaphoids that were more flexed in a neutral wrist position. (b) During wrist extension, rotation (extension) of the scaphoid increased in scaphoids that were more flexed in a neutral posture.

how scaphoid shape impacts wrist range of motion. We observed that the relative rotation between the scaphoid and capitate increased with an larger range of motion in maximum wrist flexion. We speculate that the change in shape of the concave scaphoid facet described by PC1 alters the articulation between the scaphoid and the capitate. In subjects with a high PC1 score, the scaphoid can slide past the capitate, resulting in a larger range of motion (Figure 3.6 a,b). Our results suggest that with increased wrist extension, rotation between the radius and scaphoid increases along with rotation between the scaphoid and capitate. We hypothesize that the scaphoid-capitate articulation may be affected by the change in shape of the distal pole of the scaphoid, which becomes more prominent with reduced flexion and thus may restrict scaphoid motion (Figure 3.6 c,d). This change in shape of the distal pole of the scaphoid may also limit motion between the scaphoid and capitate in ulnar deviation (Figure 3.6 e,f). Although intriguing, none of these theories can be validated with the methods described here.

While the exact mechanisms behind how changes in scaphoid shape affect wrist range of motion are not yet clear, the existence of these correlations has important implications for our understanding of the wrist. To date, changes in carpal bone kinematics have often been

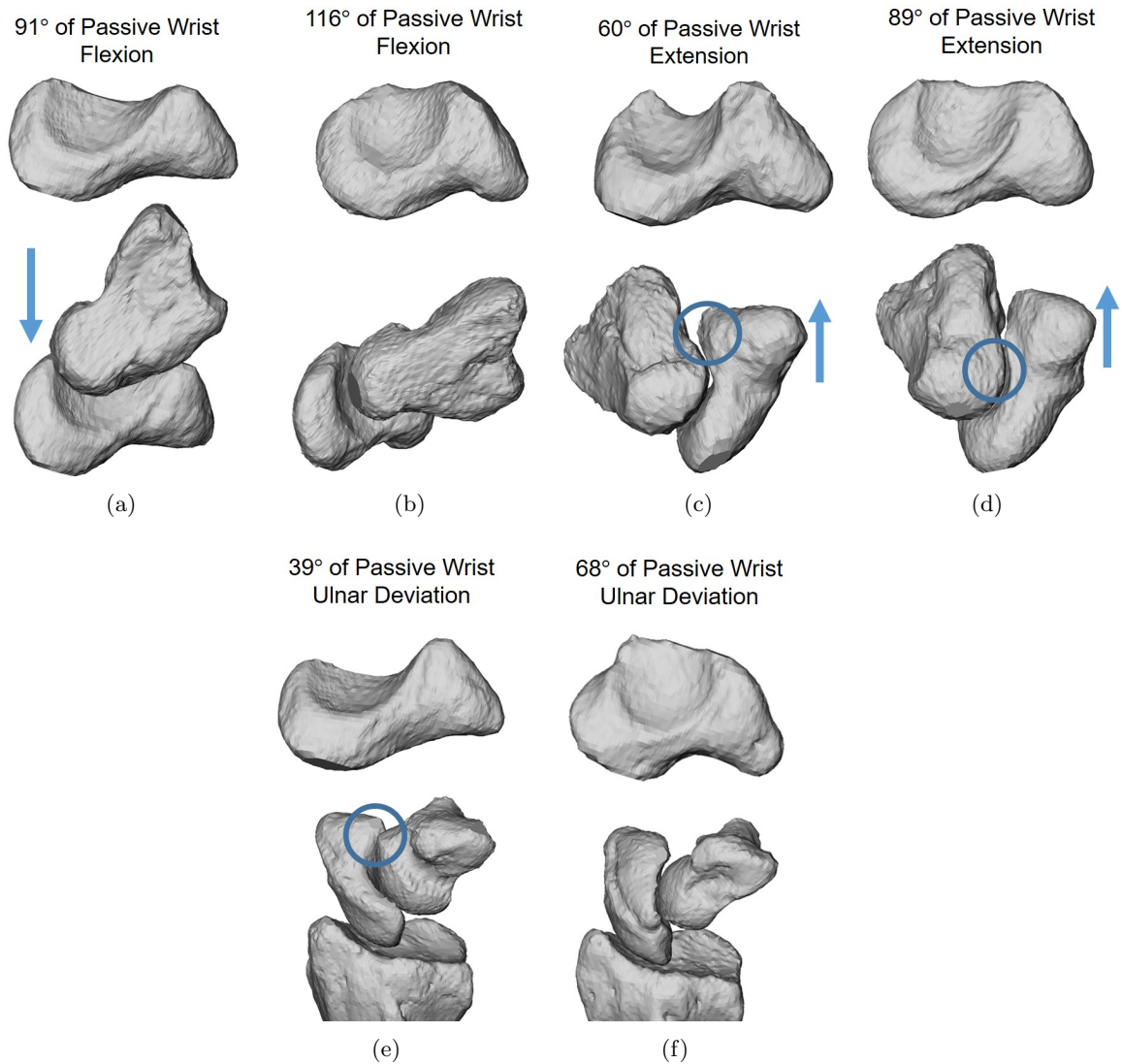


Figure 3.6: Between (a) and (b), and between (e) and (f), changes in the shape of the distal pole of the scaphoid have the potential to restrict capitate movement in wrist extension. In (c) and (d), changes in the shape of the scaphoid facet altered the relative position of the capitate, possibly limiting capitate flexion.

attributed to variation in ligamentous laxity; however, in many of these investigations, flexibility has been used as a surrogate measure for ligament properties [24], [25], [74]. Our findings demonstrate that carpal bone shape also plays a role in determining wrist flexibility. This changes our fundamental understanding of how the wrist functions. Future development of a robust musculoskeletal model of the wrist could help us to understand how

bone shape and ligament properties interact to alter wrist range of motion. For example, changes in bone shape likely affect ligament origin and insertion points.

Scaphoid posture was not correlated with any of the first five principal components of scaphoid shape, suggesting that it can be considered independently of shape. Although scaphoid posture was not correlated with passive wrist range of motion, it did influence the kinematics of the scaphoid and capitate during wrist flexion and extension. Previous work found that an increased scaphoid flexion angle was associated with a lower range of motion in active radial deviation [25], [75]. Thus, it can be suggested that scaphoid posture is an element of native carpal kinematics, and it may have some impact on wrist range of motion. In wrist flexion, we found that increased wrist range of motion was correlated with increased rotation at the scaphocapitate joint, while in extension, rotation increased between both the scaphoid and radius, and between the scaphoid and capitate.

To the best of our knowledge, no studies to date have considered how scaphoid morphology impacts wrist range of motion. Van de Giessen et al. performed principal component analysis on the scaphoid and lunate, concluding that the variation in bone shape is not statistically different from a normal distribution and that due the continuous nature of the shape mode, strict classification of these bones is not possible [69]. The modes of variation the scaphoid presented agree with our findings, where PC1 describes the height of the scaphoid waist, and PC2 describes the length of the scaphoid tubercle [69]. This method was later extended to model carpal motion patterns; however, the approach was designed to eliminate the effect of shape variation [76]. Joshi et al. developed a second method to characterize carpal bone shape, registration-based bone morphometry [77], but this has yet to be linked to variation in carpal kinematics.

One key limitation of this work is that we only have wrist range of motion and scaphoid posture data for ten subjects. Although access to additional scaphoid surfaces has allowed us to create a stable shape model, our observations could be strengthened by adding more subjects, particularly those with neutral scaphoid flexion angles between 50° and 60° . When analysing the contact area between bones, we assumed a cartilage thickness of 0.9 mm for all

subjects. We did not directly image the cartilage or account for any variation in cartilage thickness between subjects. For this analysis, we scaled the carpal bones, and did not consider the impact of carpal bone size on carpal bone motion. However, previous analysis has shown that the carpus scales isometrically as a unit, so this is unlikely to impact range of motion [54].

In summary, we have shown that scaphoid morphology plays a statistically significant role in determining wrist flexion-extension and ulnar deviation range of motion. While more work is needed to determine whether changes in morphology are causative or adaptive, our findings provide a strong link between wrist morphology and range of motion. Understanding the causes of generalized wrist laxity is a step towards understanding subject-specific variability in carpal kinematics, which may help to explain variability in patient outcomes following injury to the carpus.

Chapter 4

Discussion and Conclusions

The wrist is a highly complex joint, containing eight irregularly shaped carpal bones that are connected by a complex network of ligaments. Predicting and modelling carpal bone motion in the wrist is an important step towards understanding how the healthy wrist functions and understanding patient-specific responses to injury, but developing a theory to explain carpal bone motion is an ongoing challenge. The difficulty of this task is compounded by variability in ligament properties and carpal bone shape which impact carpal bone kinematics on a subject-specific level. Our objective was to investigate subject-specific variation in carpal bone motion and identify potential causes or effects of this variability. We performed two studies to investigate how generalized wrist laxity and carpal bone shape influence carpal bone motion.

First, we looked at carpal bone motion on the ulnar side of the wrist during a variety of functional wrist movements. We found that the lunate and triquetrum had similar motion throughout the majority of wrist movements, but there were several exceptions and motion was not always synchronous. Wrist laxity, measured using external measures of wrist flexibility, influenced the orientation of the triquetrum-radius rotation axis during motion from 20° of radial deviation to 20° of ulnar deviation. We also found that during the second phase of our hammering task, the triquetrum-radius rotation axis shifted distally with increased wrist laxity. These results show that variation in carpal bone motion is not limited to the radial side of the wrist, and can potentially help to explain variability in

patient outcomes following ligament injury.

For our second study, we used statistical shape modelling to investigate the role of scaphoid morphology as a determinant of wrist flexibility. The first principal component of scaphoid shape was found to be correlated with passive wrist flexion range of motion, while the second principal component was correlated with passive wrist extension range of motion. This suggests that external measurement of wrist flexibility may be influenced by carpal bone shape. We also found that posture of the scaphoid was independent of scaphoid shape, and while not correlated with wrist range of motion, scaphoid posture affected the amount of scaphoid rotation in wrist flexion and extension. This suggests that scaphoid posture is a property of the carpus which impacts carpal bone motion patterns in parallel with shape.

When interpreting our results, it is important to acknowledge the limitations of this work. First of all, we are unable to differentiate between causes and effects of variability in carpal bone motion using the methods described here. In the context of our first study, we cannot conclusively say whether a given carpal bone motion pattern limits range of motion, or whether a reduced range of motion favours a certain carpal bone motion pattern. Similarly, we cannot determine whether bone morphology dictates wrist range of motion, or whether the carpal bones develop to support native carpal motion patterns.

A major limitation of both investigations is the low sample size. Working with an existing database, we only had kinematic and range of motion data for 10 subjects. A larger sample size could allow for the investigation of more patterns in carpal bone motion. During our data processing, we observed several anomalies. For example, our subject with the highest laxity score had minimal carpal bone rotation in the proximal row during wrist radial-ulnar deviation. Additionally, during extreme wrist flexion, the capitate flexed relative to the scaphoid in 9 out of 10 subjects, but in one of the stiffer subjects, the capitate radial-deviated. A larger sample size has the potential to strengthen the statistical power of the work performed to date, as well as the potential to provide more representation of unique carpal motion patterns. However, we found that our sample size was sufficiently

powered to determine whether paired rotation axes had the same orientation. We also used leave one out analysis to help validate our correlations between the principal components of shape and wrist range of motion.

During these investigations, we were unable to measure ligament properties. Thus, we could not directly measure variance in ligamentous laxity, or determine whether a ligament is engaged in a specific wrist position. Previous works have used ligament recruitment as a substitution for directly measuring strain [47], [78], [79]; however, this method has several limitations. Ligament recruitment is used to predict whether a ligament is lengthening or shortening, but cannot measure force transmission, and does not consider variability in ligament stiffness. Development of a robust biomechanical model of the wrist could allow us to isolate the effects of carpal bone shape and ligamentous laxity by independently manipulating bone shape or ligament properties (such as stiffness or origin and insertion points).

Additionally, we were limited to static wrist poses, so we could not directly measure carpal bone motion between poses, and relied on interpolation. This means that we were unable to investigate the path-dependent nature of carpal bone motion; however, the hysteresis effect on carpal bone motion has been shown to be less than 2.5° [29]. During our investigation into the impact of wrist laxity on triquetrum motion, our hammering task was not along the “optimal dart thrower’s path”, with an equal ratio of flexion-extension to radial-ulnar deviation [3]. Additionally, although attempts were made to control for wrist posture during the data collection, all subjects did not reach the same positions.

Through the process of data analysis, we developed several new research questions and goals. Our finding that the rotation axis of the triquetrum shifts distally with increased wrist laxity during ulnar flexion suggests that the interaction between the triquetrum and hamate may be affected by variation in wrist laxity. As it has been proposed that the interaction between the triquetrum and hamate is crucial for rotational control of the wrist [21], it would be interesting to further analyse this interaction across other wrist movements, and investigate variation in the shape of the articular surface between the triquetrum and

hamate. Although we have identified scaphoid posture as a factor contributing to normal carpal kinematics, we still do not fully understand why scaphoid posture varies among individuals. While we could not link scaphoid posture to scaphoid shape, it is possible that the shape of surrounding bones (capitate, trapezium) could influence scaphoid posture. Further investigation could help us to understand why this variation exists, as well as identify any other effects of scaphoid posture on carpal bone motion patterns.

The findings from both studies have clinical implications with the potential to improve treatment of carpal instability. Differences in the movement of the triquetrum correlated with wrist laxity may affect the triquetrum's ability to extend the lunate. If true, this could disrupt the "balance" of the lunate [6], and help to explain differential responses to SL ligament injury and reconstruction. Additionally, the variation in the amount of relative motion between the triquetrum and lunate may help to explain variation in clinical outcomes following LT arthrodesis. The finding that the external measures of wrist flexibility are correlated with carpal bone shape is a step forwards improving our fundamental understanding of clinical laxity. Hyper laxity has been associated with wrist pain and carpal instability, but the mechanism behind the development of this instability is not yet clear. Our finding that carpal bone shape affects wrist range of motion suggests that there may be more factors contributing to generalized wrist laxity than ligament properties.

Now that we have a stronger fundamental understanding of how the wrist functions and the causes behind variability in wrist range of motion, one of our main objectives going forward is to study dynamic motion of the carpus. Using cadaveric specimens, our goal is to simulate wrist motion while tracking the carpal bones using biplanar videoradiography, allowing us to examine dynamic wrist kinematics during functional wrist movements, simulate ligament injuries to examine the effect on carpal kinematics, produce repeatable wrist movements, and determine how well surgical repairs are able to restore native carpal bone motion. This work builds upon a previous Master's project [80], which designed a working prototype of a wrist simulator. To integrate the wrist simulator with the existing equipment in the Skeletal Observation Laboratory, we replaced the electromagnetic

tracking system used in the simulator development with optical motion based-tracking, and implanted metal beads into the carpal bones to facilitate carpal bone tracking using biplanar videoradiography (Appendix A). The next steps will be to continue testing with the new testing platform. Once the equipment set-up is optimized, preliminary testing with the pilot cadaveric specimen can begin.

In the future, we are also interested in extending our investigation into the impact of scaphoid shape on carpal bone motion to look at clinical applications. During our analysis, we observed substantial variation in scaphoid shape and size. We are interested in investigating the impact of scaphoid shape on screw placement in the scaphoid following a scaphoid fracture. Future work will aim to compare optimal screw placement between scaphoids of different shapes to identify surgical challenges associated with shape variation (Appendix B). Another compelling line of investigation is to determine whether certain bone shapes are more susceptible to fracture or are associated with better surgical outcomes following fracture repair.

Finally, carpal bone shape can be investigated from an evolutionary perspective. Primates often have a different arrangement of carpal bones than humans; in some species, the scaphoid and lunate are fused or an additional bone (the os centrale) located distal to the scaphoid is present, which has been found to influence carpal kinematics [81]. Understanding how and why these changes have occurred, along with effects on range of motion, may further our understanding of how the human carpus functions.

In conclusion, we found that several factors contribute to variation in carpal bone motion between subjects. Our first study investigated the *in vivo* kinematics of the triquetrum and lunate, finding that contrary to Linscheid's intercalated segment theory [15], the lunate and triquetrum did not move in synchrony across all functional wrist movements, and the motion pattern of the triquetrum varied with generalized wrist laxity. The second study found that scaphoid shape is correlated with wrist flexion and extension range of motion. Together, these studies help us to understand variability in carpal bone motion and highlight the importance of considering subject-specific factors when restoring carpal

kinematics following injury. Our findings have the potential to lead to the improvement of surgical techniques, to allow for more accurate restoration of native carpal bone motion patterns.

Bibliography

- [1] M. J. Rainbow, “An Examination of Carpal Joint Function using Kinematic Analysis and Predictive Modeling,” PhD Thesis, Brown University, Aug. 2011.
- [2] S. W. Wolfe, J. J. Crisco, C. M. Orr, and M. W. Marzke, “The dart-throwing motion of the wrist: Is it unique to humans?” *J Hand Surg Am*, vol. 31, pp. 1429–37, Nov. 2006.
- [3] J. J. Crisco, J. C. Coburn, D. C. Moore, E. Akelman, A.-P. C. Weiss, and S. W. Wolfe, “In vivo radiocarpal kinematics and the dart thrower’s motion,” eng, *The Journal of bone and joint surgery. American volume*, vol. 87, no. 12, pp. 2729–2740, Dec. 2005.
- [4] R. A. Berger, T. Imeada, L. Berglund, and K. N. An, “Constraint and material properties of the subregions of the scapholunate interosseous ligament,” *J Hand Surg [Am]*, vol. 24, pp. 953–962, 1999.
- [5] M. J. Ritt, R. L. Linscheid, W. P. Cooney, R. A. Berger, and K. N. An, “The lunotriquetral joint: Kinematic effects of sequential ligament sectioning, ligament repair, and arthrodesis,” *J Hand Surg [Am]*, vol. 23, pp. 432–45, 1998.
- [6] M. Garcia-Elias, “Understanding Wrist Mechanics: A Long and Winding Road,” en, *Journal of Wrist Surgery*, vol. 02, no. 01, pp. 005–012, Feb. 2013.
- [7] H. K. Watson and F. L. Ballet, “The SLAC wrist: Scapholunate advanced collapse pattern of degenerative arthritis,” *J Hand Surg [Am]*, vol. 9, pp. 358–365, 1984, 3.
- [8] R. Luchetti, A. Atzei, R. Cozzolino, and T. Fairplay, “Current role of open reconstruction of the scapholunate ligament,” *Journal of Wrist Surgery*, vol. 2, pp. 116–125, May 2013.
- [9] M. P. Rosenwasser, K. C. Miyasajsa, and R. J. Strauch, “The RASL Procedure: Reduction and Association of the Scaphoid and Lunate Using the Herbert Screw,” *Techniques in Hand & Upper Extremity Surgery*, vol. 1, no. 4, pp. 263–272, Dec. 1997.
- [10] S. K. Lee, D. A. Zlotolow, S. Sapienza, R. K. Karia, and J. Yao, “Biomechanical Comparison of 3 Methods of Scapholunate Ligament Reconstruction,” *The Journal of Hand Surgery*, vol. 39, no. 4, pp. 643–650, Apr. 2014.
- [11] G. M. Best, Z. E. Mack, D. R. Pichora, J. J. Crisco, R. N. Kamal, and M. J. Rainbow, “Differences in the Rotation Axes of the Scapholunate Joint During Flexion-Extension and Radial-Ulnar Deviation Motions,” eng, *The Journal of Hand Surgery*, Jul. 2019.

- [12] S. C. Talwalkar, A. T. J. Edwards, M. J. Hayton, J. H. Stilwell, I. A. Trail, and J. K. Stanley, "Results of tri-ligament tenodesis: A modified Brunelli procedure in the management of scapholunate instability," *The Journal of Hand Surgery, European Volume*, vol. 31, no. 1, Feb. 2006.
- [13] G Blatt, "Capsulodesis in reconstructive hand surgery. Dorsal Capsulodesis for the unstable scaphoid and volar capsulodesis following excision of the distal ulna," *Hand Clin*, vol. 3, pp. 81–102, 1987.
- [14] M. A. MacConaill, "The mechanical anatomy of the carpus and its bearings on some surgical problems," eng, *Journal of anatomy*, vol. 75, no. Pt 2, pp. 166–175, Jan. 1941.
- [15] R. L. Linscheid, J. H. Dobyns, J. W. Beabout, and R. S. Bryan, "Traumatic instability of the wrist. Diagnosis, classification, and pathomechanics," *J Bone Joint Surg Am*, vol. 54, pp. 1612–32, 1972, 8.
- [16] D. M. Lichtman, J. R. Schneider, A. R. Swafford, and G. R. Mack, "Ulnar midcarpal instability-clinical and laboratory analysis," *J Hand Surg [Am]*, vol. 6, pp. 515–23, 1981, 5.
- [17] H. Moritomo, T. Murase, A. Goto, K. Oka, K. Sugamoto, and H. Yoshikawa, "In vivo three-dimensional kinematics of the midcarpal joint of the wrist," eng, *The Journal of bone and joint surgery. American volume*, vol. 88, no. 3, pp. 611–621, Mar. 2006.
- [18] M. J. Rainbow, R. N. Kamal, E. Leventhal, E. Akelman, D. C. Moore, S. W. Wolfe, and J. J. Crisco, "In vivo kinematics of the scaphoid, lunate, capitate, and third metacarpal in extreme wrist flexion and extension," eng, *The Journal of hand surgery*, vol. 38, no. 2, pp. 278–288, Feb. 2013.
- [19] A Navarro, "Luxaciones del carpo," *Anales de la Facultad de Medicina*, vol. 6, pp. 113–141, 1921.
- [20] J. Taleisnik, "The ligaments of the wrist," *J Hand Surg [Am]*, vol. 1, pp. 110–8, Sep. 1976.
- [21] E. R. Weber, "Concepts governing the rotational shift of the intercalated segment of the carpus," *Orthop Clin North Am*, vol. 15, pp. 193–207, Apr. 1984.
- [22] M. J. Sandow, T. J. Fisher, C. Q. Howard, and S. Papas, "Unifying model of carpal mechanics based on computationally derived isometric constraints and rules-based motion – the stable central column theory," en, *Journal of Hand Surgery (European Volume)*, vol. 39, no. 4, pp. 353–363, May 2014.
- [23] M. A. Craigen and J. K. Stanley, "Wrist kinematics. Row, column or both?" *J Hand Surg [Br]*, vol. 20, pp. 165–70, Apr. 1995.
- [24] M. Garcia-Elias, M. Ribe, J. Rodriguez, M. Cots, and J. Casas, "Influence of joint laxity on scaphoid kinematics," *J Hand Surg Br*, vol. 20, pp. 379–82, Jun. 1995.
- [25] G. Best, M. Zec, D. Pichora, R. Kamal, and M. J. Rainbow, "Does Wrist Laxity Influence 3d Carpal Bone Motion?" eng, *Journal of Biomechanical Engineering*, Jan. 2018.

- [26] C. J. van Andel, W. B. M. Roescher, M. Tromp, M. J. P. F. Ritt, S. D. Strackee, and D. H. E. J. Veeger, "Quantification of Wrist Joint Laxity," *Journal of Hand Surgery American*, vol. 33, no. 5, pp. 667–674, May 2008.
- [27] A. Wolff, R. Garg, A. P. Kraszewski, H. Hillstrom, J. Hafer, S. I. Backus, M. L. Lenhoff, and S. W. Wolfe, "Surgical Treatments for Scapholunate Advanced Collapse Wrist: Kinematics and Functional Performance," *Journal of Hand Surgery American*, vol. 40, pp. 1547–1553, Aug. 2015.
- [28] V. Vardakastani, H. Bell, S. Mee, G. Brigstocke, and A. Kedgley, "Clinical measurement of the dart throwing motion of the wrist: Variability, accuracy and correction," *Journal of Hand Surgery (European Volume)*, vol. 43, no. 7, pp. 723–731, Apr. 2018.
- [29] W. H. Short, F. W. Werner, M. D. Fortino, A. K. Palmer, and K. A. Mann, "A dynamic biomechanical study of scapholunate ligament sectioning," *J Hand Surg Am*, vol. 20, pp. 986–99, Nov. 1995.
- [30] C. P. Neu, R. D. McGovern, and J. J. Crisco, "Kinematic accuracy of three surface registration methods in a three-dimensional wrist bone study," eng, *Journal of Biomechanical Engineering*, vol. 122, no. 5, pp. 528–533, Oct. 2000.
- [31] B. Akhbari, A. M. Morton, D. C. Moore, A.-P. C. Weiss, S. W. Wolfe, and J. J. Crisco, "Accuracy of biplane videoradiography for quantifying dynamic wrist kinematics," *Journal of Biomechanics*, vol. 92, pp. 120–125, Jul. 2019.
- [32] M. Garcia-Elias and A. Lluch, "Partial excision of scaphoid: Is it ever indicated?" *Hand Clin*, vol. 17, pp. 687–695, Nov. 2001.
- [33] D. J. Lee and J. C. Elfar, "Carpal ligaments injuries, pathomechanics, and classification," *Hand Clinics*, vol. 31, no. 3, pp. 389–398, Aug. 2015.
- [34] D. L. Nelson, P. R. Manske, D. L. Pruitt, L. A. Gilula, and R. A. Martin, "Lunotriquetral arthrodesis," *Journal of Hand Surgery American*, vol. 18, no. 6, pp. 1113–1120, Nov. 1993.
- [35] P. M. Guidera, H. K. Watson, T. A. Dwyer, G. Orlando, J. Zeppieri, and M. Yasuda, "Lunotriquetral arthrodesis using cancellous bone graft," *Journal of Hand Surgery American*, vol. 26, no. 3, pp. 422–427, May 2001.
- [36] C. T. Atkinson and J. Watson, "Lunotriquetral Ligament Tears," *Journal of Hand Surgery American*, vol. 37, no. 10, pp. 2142–2144, Oct. 2012.
- [37] T. van de Grift and J. Ritt, "Management of lunotriquetral instability: A review of the literature," *Journal of Hand Surgery (European Volume)*, vol. 41, no. 1, pp. 72–75, Jul. 2015.
- [38] F. W. Werner, W. H. Short, and J. K. Green, "Changes in patterns of scaphoid and lunate motion during functional arcs of wrist motion induced by ligament division," *J Hand Surg Am*, vol. 30, pp. 1156–60, Nov. 2005.
- [39] F. W. Werner, J. K. Green, W. H. Short, and S. Masaoka, "Scaphoid and lunate motion during a wrist dart throw motion," eng, *The Journal of hand surgery*, vol. 29, no. 3, pp. 418–422, May 2004.

- [40] M. Garcia-Elias, X. A. Serrallach, and J. M. Serra, "Dart-throwing motion in patients with scapholunate instability: A dynamic four-dimensional computed tomography study," en, *Journal of Hand Surgery (European Volume)*, vol. 39, no. 4, pp. 346–352, May 2014.
- [41] A. Goto, H. Moritomo, T. Murase, K. Oka, K. Sugamoto, T. Arimura, J. Masumoto, S. Tamura, H. Yoshikawa, and T. Ochi, "In vivo three-dimensional wrist motion analysis using magnetic resonance imaging and volume-based registration," *J Orthop Res*, vol. 23, pp. 750–6, Jul. 2005.
- [42] J. B. Tang, J. Xu, and R. G. Xie, "Scaphoid and lunate movement in different ranges of carpal radioulnar deviation," *The Journal of Hand Surgery*, vol. 36, no. 1, pp. 25–30, Jan. 2011.
- [43] S. W. Wolfe, C. Neu, and J. J. Crisco, "In vivo scaphoid, lunate, and capitate kinematics in flexion and in extension," *J Hand Surg [Am]*, vol. 25, pp. 860–9, Sep. 2000.
- [44] F. W. Werner, W. H. Short, M. D. Fortino, and A. K. Palmer, "The relative contribution of selected carpal bones to global wrist motion during simulated planar and out-of-plane wrist motion," *J Hand Surg [Am]*, vol. 22, pp. 708–13, Jul. 1997.
- [45] T. M. Moojen, J. G. Snel, M. J. Ritt, J. M. Kauer, H. W. Venema, and K. E. Bos, "Three-dimensional carpal kinematics in vivo," *Clin Biomech (Bristol, Avon)*, vol. 17, pp. 506–14, Aug. 2002.
- [46] G. M. Best, "Scaphoid and lunate mechanics over the spectrum of healthy function," Master of Applied Science, Queen's University, Kingston ON, 2016.
- [47] M. J. Rainbow, R. N. Kamal, D. C. Moore, E. Akelman, S. W. Wolfe, and J. J. Crisco, "Subject-Specific Carpal Ligament Elongation in Extreme Positions, Grip, and the Dart Thrower's Motion," eng, *Journal of Biomechanical Engineering*, vol. 137, no. 11, Nov. 2015.
- [48] T. I. Carter, B. Pansy, A. L. Wolff, H. J. Hillstrom, S. I. Backus, M. Lenhoff, and S. W. Wolfe, "Accuracy and reliability of three different techniques for manual goniometry for wrist motion: A cadaveric study," *J Hand Surg Am*, vol. 34, pp. 1422–8, Aug. 2009.
- [49] E. L. Leventhal, D. C. Moore, E. Akelman, S. W. Wolfe, and J. J. Crisco, "Carpal and forearm kinematics during a simulated hammering task," *J Hand Surg Am*, vol. 35, pp. 1097–104, Jul. 2010.
- [50] D. Eberly, J. Lancaster, and A. Alyassin, "On gray scale image measurements: II. Surface area and volume," *CVGIP: Graphical Models and Image Processing*, vol. 53, pp. 550–562, Nov. 1991.
- [51] J. J. Crisco and R. D. McGovern, "Efficient calculation of mass moments of inertia for segmented homogeneous three-dimensional objects," *Journal of biomechanics*, vol. 31, no. 1, pp. 97–101, Jan. 1998.

- [52] J. J. Crisco, R. D. McGovern, and S. W. Wolfe, "Noninvasive technique for measuring in vivo three-dimensional carpal bone kinematics," eng, *Journal of orthopaedic research: official publication of the Orthopaedic Research Society*, vol. 17, no. 1, pp. 96–100, Jan. 1999.
- [53] J. C. Coburn, M. A. Upal, and J. J. Crisco, "Coordinate systems for the carpal bones of the wrist," *Journal of biomechanics*, vol. 40, no. 1, pp. 203–209, 2007.
- [54] M. J. Rainbow, J. J. Crisco, D. C. Moore, and S. W. Wolfe, "Gender differences in capitate kinematics are eliminated after accounting for variation in carpal size," eng, *Journal of Biomechanical Engineering*, vol. 130, no. 4, p. 041 003, Aug. 2008.
- [55] R. L. Linscheid, "Kinematic considerations of the wrist," *Clin Orthop*, pp. 27–39. Jan. 1986.
- [56] L. K. Ruby, W. P. Cooney 3rd, K. N. An, R. L. Linscheid, and E. Y. Chao, "Relative motion of selected carpal bones: A kinematic analysis of the normal wrist," *The Journal of Hand Surgery*, vol. 13, no. 1, pp. 1–10, Jan. 1988.
- [57] M. Kobayashi, R. A. Berger, L. Nagy, R. L. Linscheid, S. Uchiyama, M. Ritt, and K. N. An, "Normal kinematics of carpal bones: A three-dimensional analysis of carpal bone motion relative to the radius," *J Biomech*, vol. 30, pp. 787–93, Aug. 1997.
- [58] H. Moritomo, A. Goto, Y. Sato, K. Sugamoto, T. Murase, and H. Yoshikawa, "The triquetrum-hamate joint: An anatomic and in vivo three-dimensional kinematic study," eng, *The Journal of hand surgery*, vol. 28, no. 5, pp. 797–805, Sep. 2003.
- [59] R. N. Kamal, M. J. Rainbow, E. Akelman, and J. J. Crisco, "In vivo triquetrum-hamate kinematics through a simulated hammering task wrist motion," *The Journal of bone and joint surgery. American volume*, vol. 94, no. 12, e85, Jun. 2012.
- [60] J. J. Crisco and C. Neu, "In vivo carpal bone rotations are linear and depend on the direction of wrist rotation," in *Transactions 46th Annual Meeting Orthopaedic Research Society*, Orlando, FL: Orthopaedic Research Society, 2000.
- [61] A. K. Palmer, F. W. Werner, D. Murphy, and R. Glisson, "Functional wrist motion: A biomechanical study," *J Hand Surg [Am]*, vol. 10, pp. 39–46, Jan. 1985.
- [62] J. Y. Ryu, W. P. Cooney 3rd, L. J. Askew, K. N. An, and E. Y. Chao, "Functional ranges of motion of the wrist joint," eng, *The Journal of hand surgery*, vol. 16, no. 3, pp. 409–419, May 1991.
- [63] J. M. Kauer, "Functional anatomy of the wrist," *Clinical Orthopaedics & Related Research*, vol. 149, pp. 9–20, Jun. 1980.
- [64] K. Nakamura, M. Beppu, R. M. Patterson, C. A. Hanson, P. J. Hume, and S. F. Viegas, "Motion analysis in two dimensions of radial-ulnar deviation of type I versus type II lunates," *Journal of Hand Surgery American*, vol. 25, pp. 877–88, Sep. 2000.
- [65] R. C. Burgess, "Anatomic variations of the midcarpal joint," *J Hand Surg [Am]*, vol. 15, pp. 129–31. Jan. 1990.
- [66] M. Majima, E. Horii, H. Matsuki, H. Hirata, and E. Genda, "Load transmission through the wrist in the extended position," *J Hand Surg Am*, vol. 33, pp. 182–8, Feb. 2008.

- [67] E. Q. Pang, N. Douglass, A. Behn, M. Winterton, M. J. Rainbow, and R. N. Kamal, "Tensile and Torsional Structural Properties of the Native Scapholunate Ligament," eng, *The Journal of Hand Surgery*, Feb. 2018.
- [68] A. L. Clouthier, C. R. Smith, M. F. Vignos, D. G. Thelen, K. J. Deluzio, and M. J. Rainbow, "The effect of articular geometry features identified using statistical shape modelling on knee biomechanics," eng, *Medical Engineering & Physics*, vol. 66, pp. 47–55, Apr. 2019.
- [69] M. van de Giessen, M. Foumani, G. J. Streekstra, S. D. Strackee, M. Maas, L. J. van Vliet, K. A. Grimbergen, and F. M. Vos, "Statistical descriptions of scaphoid and lunate bone shapes," *Journal of Biomechanics*, vol. 43, pp. 1463–1469, Feb. 2010.
- [70] D. C. Moore, J. J. Crisco, T. G. Trafton, and E. L. Leventhal, "A digital database of wrist bone anatomy and carpal kinematics," eng, *Journal of biomechanics*, vol. 40, no. 11, pp. 2537–2542, Feb. 2007.
- [71] A. Myronenko and X. Song, "Point set registration: Coherent point drift," *IEEE transactions on pattern analysis and machine intelligence*, vol. 32, no. 12, pp. 2262–2275, Mar. 2010.
- [72] L. Mei, M. Figl, D. Rueckert, A. Darzi, and P. Edwards, "Sample sufficiency and number of modes to retain in statistical shape modelling," *Medical image computing and computer-assisted intervention: MICCAI ... International Conference on Medical Image Computing and Computer-Assisted Intervention*, vol. 11, pp. 425–433, 2008.
- [73] G. E. Marai, D. H. Laidlaw, C. Demiralp, S. Andrews, C. M. Grimm, and J. J. Crisco, "Estimating joint contact areas and ligament lengths from bone kinematics and surfaces," eng, *IEEE transactions on bio-medical engineering*, vol. 51, no. 5, pp. 790–799, May 2004.
- [74] M Garcia-Elias and C Orsolini, "Relationship between thumb laxity and trapezium kinematics," eng, *Chirurgie de la main*, vol. 30, no. 3, pp. 224–227, Jun. 2011.
- [75] Y Minamikawa, C. A. Peimer, T. Yamaguchi, J. Medige, and F. S. Sherwin, "Ideal Scaphoid Angle for Intercarpal Arthrodesis," *Journal of Hand Surgery American*, vol. 17, no. 2, pp. 370–375, Mar. 1992.
- [76] M. van de Giessen, M. Foumani, F. M. Vos, S. D. Strackee, M. Maas, L. J. van Vliet, C. A. Grimbergen, and G. J. Streekstra, "A 4D Statistical Model of Wrist Bone Motion Patterns," *IEEE Transactions on Medical Imaging*, vol. 31, no. 3, pp. 613–625, Mar. 2012.
- [77] A. A. Joshi, R. M. Leahy, R. D. Badawi, and A. J. Chaudhari, "Registration-Based Morphometry for Shape Analysis of the Bones of the Human Wrist," *IEEE Transactions on Medical Imaging*, vol. 35, no. 2, pp. 416–426, Feb. 2016.
- [78] E. Halilaj, M. J. Rainbow, D. C. Moore, D. H. Laidlaw, A.-P. C. Weiss, A. L. Ladd, and J. J. Crisco, "In vivo recruitment patterns in the anterior oblique and dorsoradial ligaments of the first carpometacarpal joint," *Journal of Biomechanics*, vol. 48, no. 10, pp. 1893–1898, Jul. 2015.
- [79] L Blankevoort, R Huiskes, and A de Lange, "Recruitment of knee joint ligaments," *Journal of Biomechanical Engineering*, vol. 113, no. 1, pp. 94–103, Feb. 1991.

-
- [80] M. C. Pearson, “An Open-Source Device for Tendon Actuated Wrist Motion,” Master of Applied Science, Queen’s University, Kingston ON, Sep. 2017.
- [81] C. M. Orr, “Kinematics of the anthropoid os centrale and the functional consequences of scaphoid-centrale fusion in african apes and hominins,” *Journal of Human Evolution*, vol. 114, pp. 102–117, Jan. 2018.
- [82] E. L. Leventhal, S. W. Wolfe, E. F. Walsh, and J. J. Crisco, “A computational approach to the ”optimal” screw axis location and orientation in the scaphoid bone,” *The Journal of Hand Surgery*, vol. 34, no. 4, pp. 677–684, Apr. 2009.

Appendix A

Simulated Wrist Motion Using Cadaveric Specimens

A.1 Optical Motion Tracking

3D printed clusters were designed to mount optical motion capture markers on the radius and third metacarpal. (Figure A.1). Each cluster consists of two pieces, which are glued around a 3 mm countersunk screw inserted into the bone of interest.

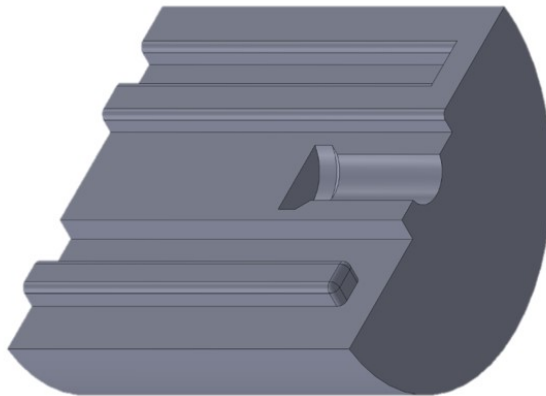


Figure A.1: 3D printed clusters are used for mounting optical tracking markers.

For future testing, a more anatomically accurate 3D printed replica of the cadaveric specimen has been created from a CT scan of the hand and forearm (Figure A.2).

Similar to the existing testing platform, it uses a ball and socket joint with to simulate wrist motion. This new testing platform can either be mounted directly to the simulator base, similar to the existing platform, or it can be integrated with the specimen mount, using

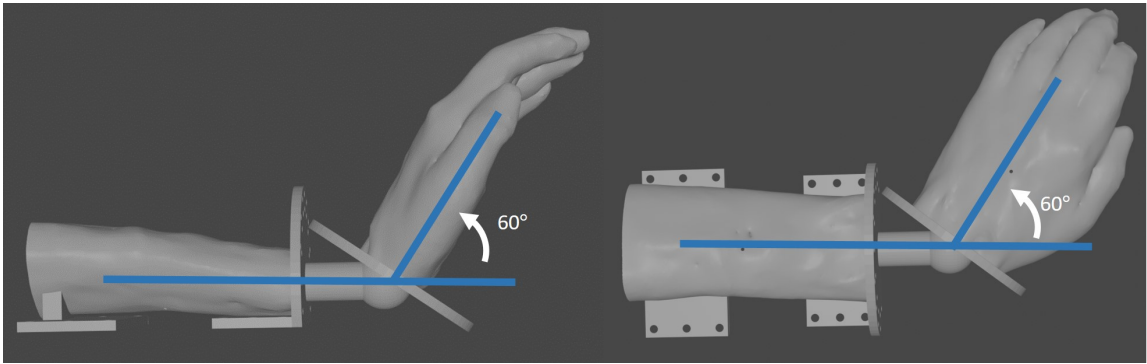


Figure A.2: Computer-generated model of the cadaveric specimen with ball and socket joint at the wrist, showing the range of motion at the joint.

Schanz pins screwed into the plastic to hold the forearm in place. On the new platform, the mount for the ball and socket joint was elongated, to allow for an increased range of motion at the wrist compared to the original testing platform. The tracking clusters can be directly mounted on to the 3D printed test apparatus (Figure A.3), and can be easily repositioned if needed. This new platform is designed to facilitate future testing to determine the optimal position of the marker clusters, motion capture cameras, and biplanar videoradiography equipment without the use of biohazardous material.

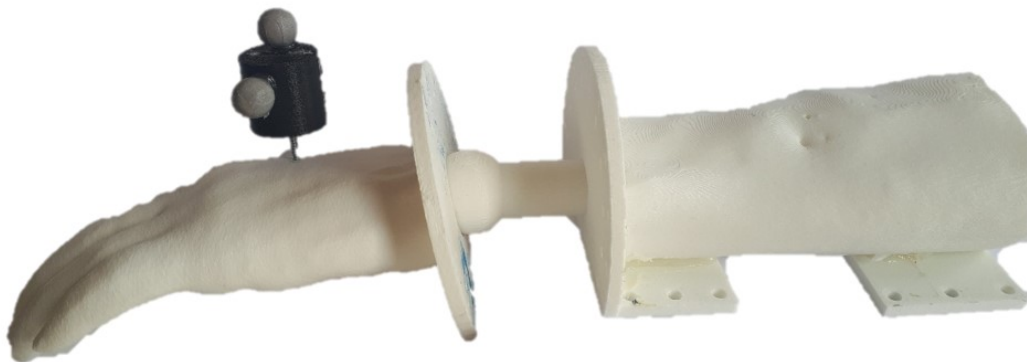


Figure A.3: 3D printed replica of the cadaveric specimen with tracking cluster mounted at the approximate location of the third metacarpal.

A.2 Bead Implantation

For accurate tracking of the carpal bones during dynamic movements using biplanar videoradiography (BVR), the decision was made to implant small metal beads into the carpal bones. By implanting three beads into each of the carpal bones, the location of the beads can be identified and tracked in the x-ray videos. Although it is possible to track bone position with the use of metal beads, inserting the beads allows for more accurate tracking, particularly in the carpus, since having many bones in a small space may result in occlusion. Through an iterative process, a procedure was designed to implant beads into the carpal bones while minimizing disruption to the joint capsule and minimizing incorrect bead placement. The finalized bead implantation procedure is summarized below.

A.2.1 Bead Implantation Procedure

Materials

- 18 gauge needles
- 1 mm radiopaque beads
- cyanoacrylate (superglue)
- paper clips or stiff 0.8 mm wire

Apparatus

- Dremel
- 1 mm drill bit
- Dremel cut off wheel
- small hammer or mallet
- forceps
- scalpel
- tweezers

Preparation

1. Ensure that you are familiar with the anatomy of the specimen. Palpation videos for the targeted bones can be helpful. This is critical for helping you to locate the bones of interest.
2. Break off the plastic sheaths from the needles. This can be done using the Dremel with the cut off wheel attachment while holding the needle tips with the forceps. Take

care not to crush the needle. Generally, try to cut as close to the plastic as possible to preserve the longest needle, but some varied lengths can also be useful. For stronger bones (ex: the radius or ulna), ensure that the needle sheath is shorter than the drill bit. This allows the needle and drill bit to be used as a cannulated drill.

CAUTION: both ends of the needle will be sharp. Handle with forceps whenever possible.

3. Straighten the paper clips, leaving a bent portion to act as a handle. Test that each paper clip fits through the needles, so it is able to act as a ramrod.
4. Perform warm-up procedure for x-ray system.
5. Prepare x-ray volume by covering the specimen placement area with tarp or other barrier.

Implantation Procedure

NOTE: It is helpful to have two individuals so that one person can work directly with the specimen, while the other operates the x-ray equipment.

1. Prepare the workspace. Gather all listed equipment and ensure it is easily accessible, to minimize contact with storage areas once you are working with biohazardous material. Retrieve the specimen.
2. (optional) Place the beads on a soft surface (ex: a clean rag), as this makes them easier to pick up using the forceps.
3. Palpate the bone of interest. Flexing and extending the wrist can help distinguish between the carpals and the distal forearm (the carpal bones will move, while the radius and ulna are relatively stationary).
 - If you are struggling, use the scalpel to make a midline, sagittal incision (about 5-10 cm long) on the dorsal side of the carpus, through the skin and connective tissue. Take care not to damage the tendons or joint capsule. This is helpful for locating the carpal bones and avoiding tendon damage, as you do not have to palpate through the skin. Repeat on the volar side if needed.
4. Insert the needle into the targeted bone. Take care to avoid inserting the needle into any tendons.
 - For weaker bones (carpals): once the bone has been located, grasp the needle with the forceps, and stab the needle into the bone. If necessary, use a hammer or mallet to ensure the needle has good purchase in the bone.
 - For stronger bones (radius, ulna, some carpals), it may not be possible to securely insert to the needle using pressure from the forceps or the hammer. In this case, place the needle in the desired location, and grasp firmly with the forceps. Insert

the drill bit into the needle, and then drill into the bone. You will be able to feel the drill penetrate the cortical bone shell. Remove the drill bit, while pushing down on the forceps to push the needle into the hole. If needed, use the hammer to tap the needle into the bone.

5. Manually check the needle position. When manual pressure is applied to the forceps, the needle should feel firm, and should not wiggle if perturbed. To test you are in the targeted bone, manipulate the specimen and ensure the needle follows the expected motion of the targeted bone. For example, during wrist radial-ulnar deviation, the scaphoid would be expected to flex and extend, while the capitate would radial-ulnar deviate.

6. Check the needle position using x-ray. Remove the forceps and transport the specimen to the x-ray volume. Take an x-ray and then consult the image to see if the needle is in the expected location.

NOTE: This this might seem time consuming, but is VERY helpful in preventing floating beads and ensuring every targeted bone has beads implanted. I would recommend using imaging the specimen every time a bead or needle is inserted. If you find you are in the wrong bone, leave the needle in and use it as a reference for another attempt. Remove any needles not in a bone as they move and are not a reliable reference.

7. Insert the bead.

- (a) Check the needle has not moved during transport and is still firmly in place. Reattach the forceps.
- (b) (optional) Grasping the forceps, drill slightly into the bone, stopping once you feel pressure. This step ensures that the bead penetrates the targeted bone; however, for smaller carpal bones, it is possible to drill through the bone.
- (c) Use the tweezers to pick up a bead a drop it into the needle.
- (d) Use a paper clip to push the bead down the needle, into the bone.
- (e) Insert a drop of cyanoacrylate into the needle. Using the paper clip, push the glue down the needle, into the specimen.
- (f) Grasp the forceps and pull upwards on the needle while pushing down on the paper clip, so that the needle sheath slides over the paper clip. This simultaneous movement ensures that bead does not remain wedged in the needle sheath.
- (g) Remove the needle and paper clip. Check the tip of the needle sheath and the paper clip to ensure the bead is not stuck to the insertion apparatus.
- (h) Inspect the needle and paper clip. Ensure both are free of excess glue, and that the paper clip is straight. If so, they can be reused; otherwise, dispose in a secure sharps container.

8. Check the bead placement. Transport the specimen to the x-ray volume and image the specimen to confirm that the bead is in the desired location.

9. Repeat until the desired number of beads have been inserted.

Appendix B

The Impact of Scaphoid Morphology on Screw Placement in the Scaphoid

B.0.1 Modelling Procedure

From a shape atlas of 24 scaphoid surfaces, we applied principal component (PC) analysis to all 24 scaphoid meshes to create a statistical shape model independent of alignment as described in Chapter 3. For this analysis, we did not scale the scaphoids, as we wanted to investigate the impact of scaphoid size on screw placement. For our preliminary analysis, we considered the first two principal components for further analysis, which explained 39% and 18% of the variation in shape, respectively. Using our principal component scores, we generated 16 simulated scaphoids for each principal component, ranging from +3SD to -3SD of the mean score (Figure B.1). This allowed us to consider the influence of each principal component separately and investigate a wide range of shapes that may not be represented in our sample.

B.0.2 Safe Zone Calculation

To determine the optimal screw placement, we used the maximal screw length technique described in [82]. For each of the simulated scaphoids, we began by identifying a “safe zone” for screw placement. As per previous work, this was defined as a 3D dimensional surface with 2.3 mm of the cortical bone surface, to accommodate a 1.7 mm screw assuming a 0.36 mm cortical bone thickness with a 0.25 mm safety margin [82]. Calculations were

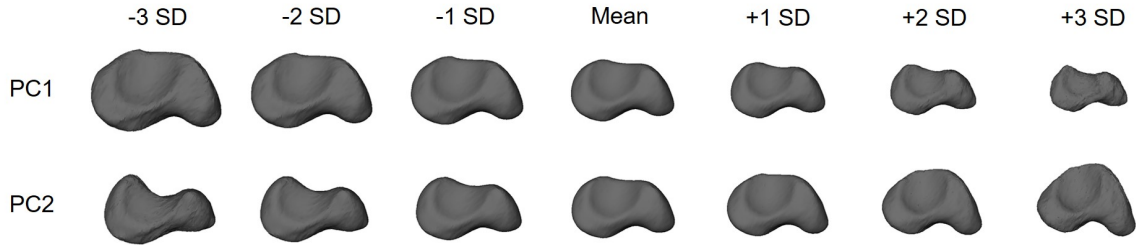


Figure B.1: Simulated scaphoids showing three standard deviations of shape for the first two principal components. Principal component one scales the scaphoid, while principal component two changes the width of the waist of the scaphoid.

performed in MATLAB and the resulting safe insertion zones were smoothed in Geomagic Wrap to refine any holes or discontinuities in the surface mesh (Figure B.2a).

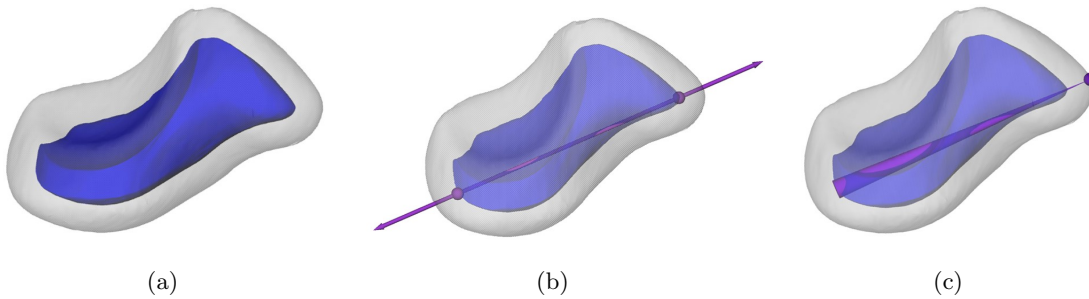


Figure B.2: (a) Image of the outer shell (grey) and the inner safe screw insertion region (blue) located 2.3 mm inside the outer shell for the mean scaphoid shape. (b) The screw axis was computed as the longest axis entirely enclosed within the safe insertion region. (c) For sensitivity analysis, a cone is used to simulate variation in the axis trajectory. For illustrative purposes, the aperture of the cone has been set to 5 degrees. In this case, the cone pierces the safe insertion zone.

B.0.3 Optimal Screw Placement

To determine the optimal orientation and location of the screw axis, we used the maximal screw length approach described in [82], as it was found to produce superior results to a second approach – using the long axis of a cylinder fitted to the safe zone. Custom code was written in MATLAB to determine the longest possible axis that could be entirely contained within the safe insertion zone described above for each of the simulated scaphoids (Figure B.2b). For all screw placements, sensitivity analysis was performed to determine

how sensitive the optimal screw placement was to errors in screw trajectory. The intersection point between the screw axis and the outer bone shell was identified at the screw intersection site, the distal pole of the scaphoid. Then, a cone was constructed with this intersection point as the apex and a base at the intersection of the screw axis and the safe zone at the proximal scaphoid. Working in a circle in 5° increments, the intersection between this cone and the safe zone was identified, and an axis was constructed between this intersection point and the apex of the cone, representing a screw placement with a trajectory error equal to the aperture of the cone (Figure B.2c). If this axis is contained within the safe zone, this screw placement is acceptable. The aperture of the cone is then increased until all axes for a given aperture are no longer contained in the safe screw insertion volume.

B.0.4 Cross-sectional Area

As an additional metric to measure the difficulty of screw placement, the minimal cross-section area of the safe zone through the waist of the scaphoid was identified for each of the simulated scaphoids. In MATLAB, a series of planes perpendicular to the screw axis were constructed, and the intersection between the “safe zone” and each plane was identified using to produce a two-dimensional shape (Figure B.3). For each simulated scaphoid, the slice with the minimum area was identified as the local minimum of slice area versus distance along the screw axis. For scaphoids without a well-defined waist and no local minimum, the minimum area of the scaphoid waist was taken as the plane with the gradient closest to zero. For each set of 16 simulated scaphoids, the volume of the safe insertion zone, the minimum slice area, and the length of the optimal screw were compared to the principal component score.

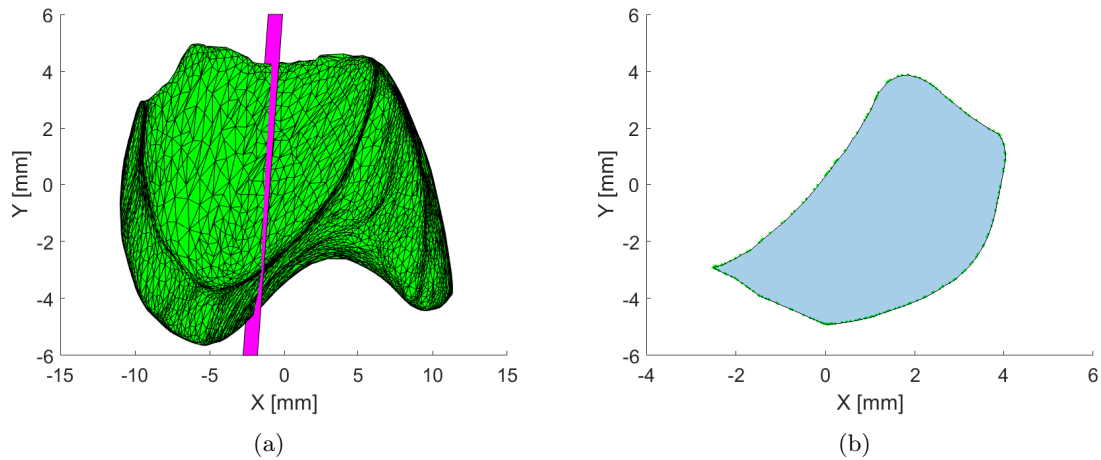


Figure B.3: Cross-sectional area of the safe insertion zone was computed for a series of plane perpendicular to the screw axis. (a) A sample plane and (b) the corresponding region of intersection.

B.1 Preliminary Results

B.1.1 Principal Component 1: Scaphoid Size

The first principal component, responsible for 39% of the variation in scaphoid shape, was isometric scaling. From the largest to the smallest simulated scaphoid, the length of our optimally placed screw (Figure B.4) dropped by 16.5 mm, a decrease of 56% (Figure B.5). The volume of the safe zone for screw insertion decreased by 95% between the largest and smallest simulated scaphoids (Figure B.6), and the minimum slice area decreased by 89% (Figures B.7 and B.8).

B.1.2 Principal Component 2: Scaphoid Shape

The second principal component describes the width of the scaphoid waist and is responsible for 18% of the shape variance in the scaphoid. As the width of the scaphoid waist increased, the length of the optimally placed screw decreased. Over three standard deviations, this decrease was equal to 4 mm, or 17% of the screw length (Figure B.5). The safe volume for screw insertion also decreased with an increase in the width of the waist of the scaphoid from 589 mm^3 to 449 mm^3 (24%) (Figure B.6). The minimum cross-sectional area of the

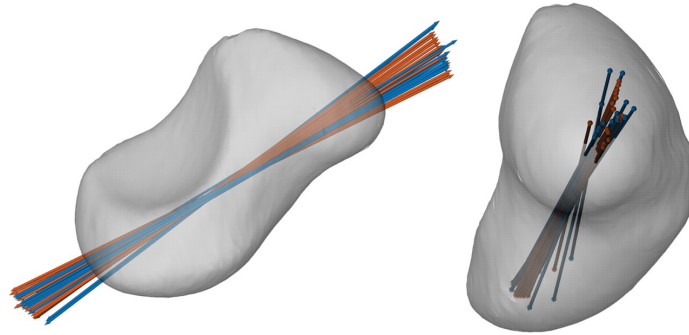


Figure B.4: Location and orientation of the screw axis for 32 simulated scaphoids, overlaid on the mean shape. Axes corresponding to simulated scaphoids generated using PC1 are shown in blue, while those corresponding to PC2 are shown in orange.

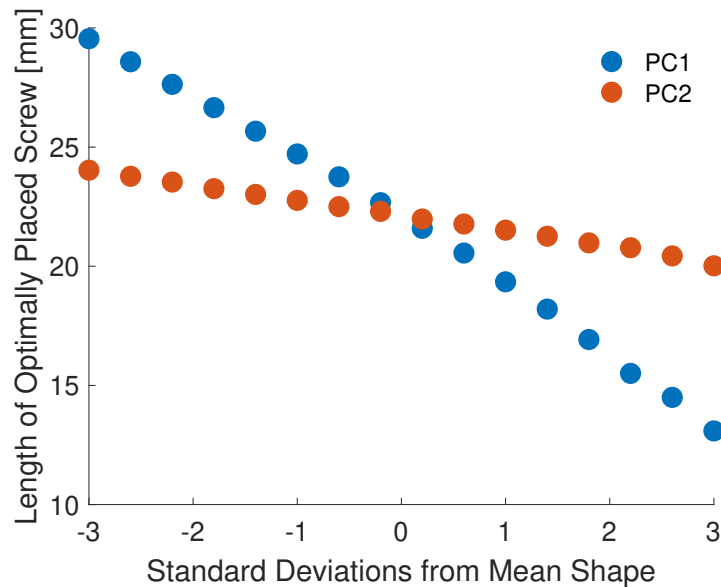


Figure B.5: Length of the optimally placed screw for 16 simulated scaphoids representing the first two modes of variation. For both principal components, positive deviation from the mean was associated with a shorter screw length

simulated scaphoids varied by 5 mm^2 (Figures B.7 and B.8). The minimum cross-sectional area was found to be larger in shapes closer to the mean, and then decrease as the shape approached the extremes.

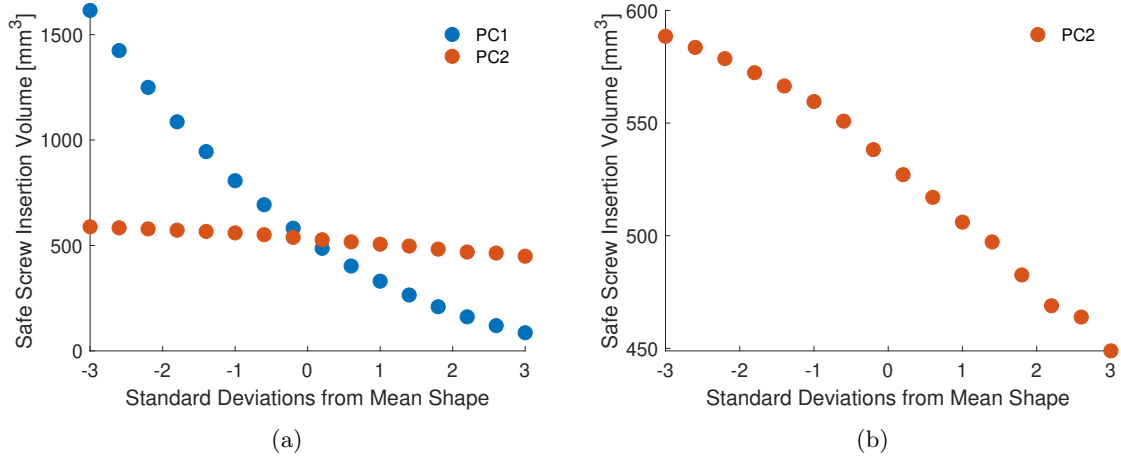


Figure B.6: For both principal components, positive deviation from the mean shape led to a decrease in the safe screw insertion volume; however, altering PC1 led to greater variation in the safe insertion volume than PC2.

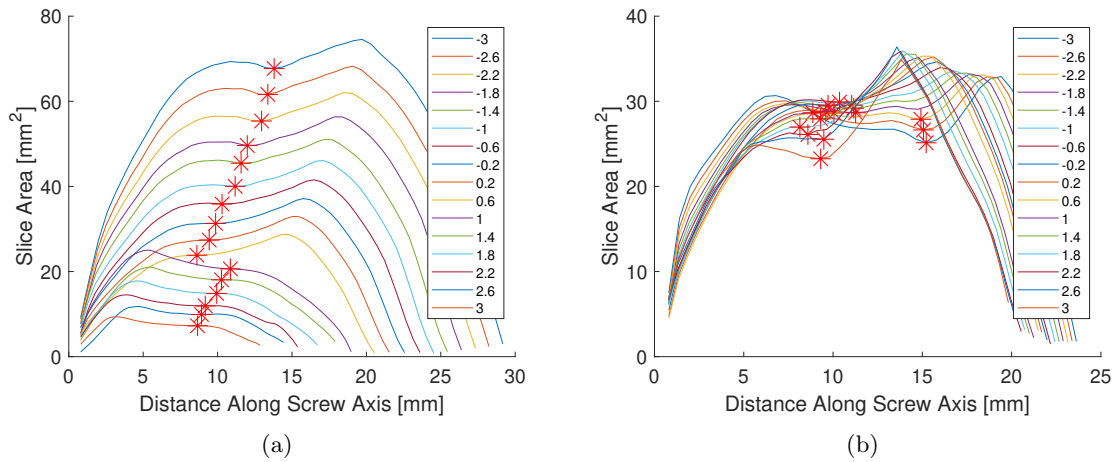


Figure B.7: 2D area of the safe insertion zone along the screw axis for all simulated scaphoids, identified by their standard deviation score for (a) PC1 and (b) PC2. The minimum slice area of the scaphoid waist is indicated with a red asterisk.

B.1.3 Sensitivity

All screw axes found using our optimization technique were found to be highly sensitive to screw trajectory. In all cases, less 1° of error in trajectory caused the screw to penetrate the safe zone.

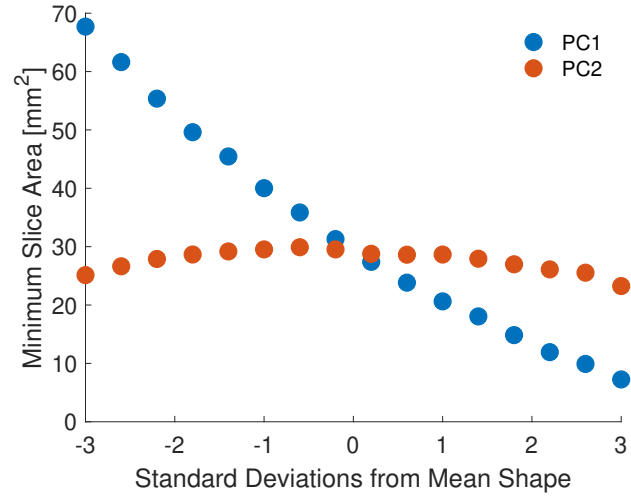


Figure B.8: Changes in scaphoid morphology due to the first two principal components affected the minimal cross-sectional area (indicated by a red asterisk in the shape profiles in Figure B.7) of the safe insertion zone through which the optimal screw passed.